Rotational Friction Kernel in Water from the Femtosecond Time-Resolved Optical Kerr Effect of Acetonitrile/Water Mixtures

Niko P. Ernsting,* George M. Photiadis,† Horst Hennig, and Thomas Laurent

Department of Chemistry, Humboldt University, Brook-Taylor-Strasse 2, D-12489 Berlin, Germany

Received: May 3, 2002; In Final Form: July 8, 2002

Depolarized Rayleigh scattering (DRS) of acetonitrile/water mixtures is examined with the time-resolved, heterodyne-detected optical Kerr effect (OHD-OKE). For neat water, the rise of electronic response gives a symmetric apparatus function and an asymmetric correction is constructed with the help of high-frequency Raman data. For the mixtures at 21 °C, depolarized Raman spectra up to 1600 cm^{-1} are obtained with high signal/noise ratio. The DRS spectra for acetonitrile mole fraction $0.05 \le x_{\mathrm{ACN}} \le 1$ are decomposed into the spectra of water and of neat acetonitrile and a "composite" spectrum with associated weight functions. The spectral density at infinite dilution in water is obtained by extrapolation and transformed into the second-rank orientational correlation function of single acetonitrile solutes. The Einstein frequency of 31.11 cm^{-1} is higher than the value of 27.11 cm^{-1} for the potential-free stochastic rotor and an oscillation is observed in the corresponding velocity correlation function, both indicating librational motion in a solvent cage. The rotational correlation time $\tau_2 = 1.49 \pm 0.015$ ps may be used to rescale τ_2 values from ^{14}N nuclear quadrupole relaxation in water; the comparison provides an improved value 4.54 ± 0.03 MHz for the coupling constant. The correlation function is inverted to give the kernel for rotational friction. The latter consists of a fast biexponential decay with a 33-fs correlation time followed by exponential decay with a 0.779-ps time constant. An oscillatory residue around 0.3 ps indicates coupling between acetonitrile libration and the water frictional modes.

Introduction

The characterization of intermolecular interactions in liquids is important for an understanding of the role that the solvent plays in condensed-phase chemical reactions. The solvent affects the ease with which reactants approach or products separate and thereby controls the rate and efficiency of many chemical reactions. During the reactive step the solvent acts as a bath that can either supply thermal energy or accept excess energy, because nearby solvent molecules exert fluctuating forces and so influence the motion along the reaction coordinate.[1] The nature of this friction—its mechanism, strength, and effect—may also be examined with the nonreactive motion of suitable probes in solution. With this purpose, theoretical interest and recent femtosecond experiments focused on elementary molecular processes such as reorientation[2−4] and vibrational relaxation,[5−10] mostly in nonpolar fluids, since here forces on a molecular solute are due to short-range interactions and their fluctuations arise from solvent translational motion only,[11] paving the way for stochastic or collisional modeling.

The temporal behavior of the frictional forces determines the coupling to the solute motion, but it also reflects on the way the process is described. To see this, imagine a model for the motion constructed from all relevant modes (the system) which may be time-resolved by an experiment at hand. In this case the remaining modes (the bath) contribute force fluctuations which can be assumed to be δ-correlated in time, i.e., instantaneous friction. On the other hand, one may want to describe the observations with a simpler model which provides better direct insight. For example, solute reorientation may be modeled as free rotation, i.e., without potential energy. Then some of the dynamics will not be captured explicitly and instead is viewed as an external force which fluctuates with some time structure or memory. In this case the system dynamics is governed by a generalized Langevin equation (GLE), which now includes time-dependent friction.[12−15] The latter therefore indicates that the present system is not complete. Seen in a different way, finding time-dependent friction points to an additional interaction with the solvent that is neglected by the model. In this paper we report the measurement of time-dependent friction for rotation of a small molecular probe in water and find indications of solvent caging.

Polar solvents owe most of their properties to orientational structure and dynamics and possibly to H-bonding. When a charge is redistributed during a chemical reaction in a polar solvent,[16] it feels not only near-range friction but also forces from polar interactions with solvent molecules which may be further away. In most cases the solvent polarization can adjust to, and follow, the instantaneous charge distribution so that the reaction runs in a mean solvent field. However, if the driving process is faster, then the solvent polarization may lag behind and so decelerate the reaction. These ideas were applied by Nee and Zwanzig in their seminal 1970 paper[17] to the rotation of a dipolar solute in a cavity surrounded by a dielectric continuum. The rotational friction due to the continuum was calculated from the dielectric dispersion and termed "dielectric". A purely molecular perspective was reached in 1982 by Madden and Kivelson,[18] who approached dipolar solute rotation including inertial motion from the torque fluctuations. They assumed that short-range and dipolar frictional torques are not time-correlated and later specialized to the limit for rotational diffusion. Their

---

* E-mail: nernst@chemie.hu-berlin.de.

† On leave from the Institute of Chemical Engineering and High-Temperature Chemical Processes-FORTH and Department of Chemical Engineering, University of Patras, P.O. Box 1414, GR-26500, Patras, Greece.

10.1021/jp0260649 CCC: $22.00

dielectric friction kernel (eq 53 in ref 18a) consists of several exponential terms with time constants made up from transverse (τ_D) and longitudinal (τ_D/ϵ_0) Debye relaxation times together with the near-range rotational diffusion coefficient D_0; these terms are modified by translational motion of the solute and thereby made faster. Theories of dielectric rotational friction and the field up to 1994 were reviewed in a molecular dynamics study by Papazyan and Maroncelli[19] to which the reader is referred for earlier contributions. Recent advances have come from molecular dynamics (MD) simulations of dipolar rotation of small model solutes,[20,21] which we will discuss in this paper. Simulations were also used to analyze the effect of dielectric friction on ion mobility[22−26] and on vibrational dephasing and relaxation of a molecular solute.[6,7,27−33]

Experiments to detect or measure dielectric friction mostly proceeded from the predictions for dipolar rotation. In this context recall that spectroscopies are distinguished by the rank L of the underlying orientational correlation function ($L = 1$ for dielectric relaxation, FIR, IR; $L = 2$ for NMR, depolarized Rayleigh scattering DRS or the time-resolved optical Kerr effect OKE, Raman, optical dichroism).[34] Furthermore a spectroscopic bulk property is the result of from many molecules, and its correlation function therefore consists of molecular self-correlation and cross-correlation terms. IR, NMR, and Raman measurements address primarily intramolecular bonds with little correlation between different molecules; this is why these spectroscopies are said to have single molecule character. On the other hand, dielectric relaxation, FIR, DRS or OKE, and optical dichroism are sensitive to the relative orientation of nearby molecules, hence they have collective character.[35] NMR methods, notably nuclear quadrupole relaxation (NQR), do not rely on distinct solutes and therefore can examine neat liquids. Time-resolved optical dichroism of molecular probes returns a collective signal, so in order to conform to the model requirements, one needs a low concentration in the liquid—mostly dyes which are excited in the visible. Common to both techniques is that they provide[36] a second rank rotation correlation time τ_2 which is given by the time integral of the friction, i.e., the friction constant. This integral measure is dominated by instantaneous (near-range or hydrodynamic) friction, while the dielectric part should contribute ~10%. Hence to obtain the latter, the former must be determined independently to ~1%. In the optical realm this problem was tackled by comparing rotational dynamics for ground and excited electronic states of the chromophore[37,38] or by exploiting connections to solvation dynamics,[39] but the results provided insight into the dye/liquid interaction[40,41] rather than the desired solvent property alone. Other attempts to characterize dielectric effects on rotational dynamics included a change of probe charge,[42] comparison of dyes with similar structure[43−45] or different H-bonding,[46−49] and systematic variation of solvent viscosity[50−52] or ion strength.[49,53,54] With NMR techniques the molecular probes may be simpler but instantaneous friction must be transferred from nonpolar solvents[55] which may not meet the required accuracy. We are not aware of an unequivocal measurement of the dielectric rotational friction constant, let alone friction kernel, for a polar liquid.

Here we report on time-dependent rotational friction in water using dipolar acetonitrile, CH_3CN, as a probe. The importance of water as solvent for charge-transfer reactions need hardly be emphasized.[56] Acetonitrile was suggested in ref 19 because the probe should rotate on a time scale similar to the solvent to be able to distinguish between instantaneous and slow-relaxing friction. This was followed by MD simulations of neat acetonitrile[21] with the intriguing result that near-range and dielectric friction *cannot* be separated in principle, contrary to previous assumptions. The same conclusion had been reached in an MD simulation of acetonitrile in water,[20] which, however, examined mainly the influence of solute polarizability on the friction dynamics. The coupling of near-range translational and rotational friction is illustrated in Figure 1 which shows the polar solute surrounded by H_2O solvent molecules. Thermal rotational motion of an H_2O which is far away (b) produces a frictional torque on the solute only by coupling with its dipole field. For an H_2O nearby (a), however, its rotation may generate an additional torque by impact of atoms onto the repulsive wall of the solute. With the simulations at hand we wish to obtain equivalent experimental data for comparison. Because CH_3CN has significant polarizability anisotropy while H_2O does not (Table 1), the time-resolved optical Kerr effect with optical-heterodyne detection (OHD-OKE)[72−75] is the method of choice to observe solute orientational dynamics. We note in passing that it is equivalent to frequency-domain DRS.[76,77] However with OHD-OKE one can access the region below 50 cm^{-1} which with DRS is masked by the intense quasi-elastic Rayleigh−Brillouin scattering peak. For good measure we shall examine the entire compositional range of acetonitrile/water mixtures, which is of interest by itself in connection with the concept of microheterogeneity,[78] and then extrapolate to infinite dilution.

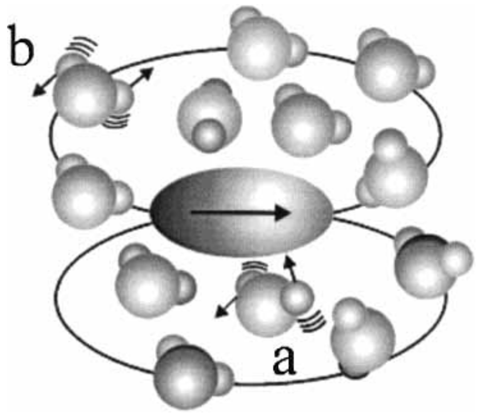

Figure 1. Torque fluctuations experienced by an acetonitrile solute due to rotation of solvent water molecules. The rotation of an H_2O far away (b) couples by dipolar interaction. The rotation of an H_2O nearby (a) may generate an additional torque by impact of atoms onto the repulsive wall of the solute—translational and rotational friction are not separable.[21]

The organization of the paper is as follows. After an Experimental Section we present three results. The first concerns the DRS spectrum of water,[79,80] which is needed for reference. In obtaining this spectrum we develop a novel technique to determine the temporal apparatus function. The second result is an improved DRS spectrum of pure acetonitrile, which has been measured before.[63,81−87] The spectra of the various mixtures are reported in the third part, analyzed by mole-weighted fitting, and extrapolated. The discussion focuses on the DRS spectrum of dilute acetonitrile in water from which the friction kernel is extracted. The dependence of integral spectral properties with acetonitrile mole fraction is examined in the final part of the discussion, followed by conclusions.

Experimental Section

A Ti:Sa laser oscillator (femtolaser) produces 400 mW average power in pulses of 14 fs fwhm. The beam is expanded and routed through a prism compressor. After that, 10% reflection from a beam splitter (Rh-sputtered quartz plate,

TABLE 1: Gas Phase (Italics) and Liquid Properties of Acetonitrile and Water Pertinent for the Analysis of OKE Traces[a]

		CH_3CN	H_2O
density	ρ, mol l^{-1} (298.15 K)	18.919[e]	55.344[e]
moments of inertia	I_A, 10^{-40} g cm^2	*5.4*[m]	*1.009 03*[j]
	I_B, 10^{-40} g cm^2	*91.2*[h,m]	*1.927 67*[j]
	I_C, 10^{-40} g cm^2	*91.2*[h,m]	*3.017 19*[j]
diffusion constant in water	D, 10^{-5} cm^2 s^{-1}	1.8[o]	2.3,[o] 2.23[n]
dipole moment	μ, D	3.9,[b] 3.94,[c] *1.54* au[g]	1.8,[b] 1.84[c]
dielectric constants	ϵ_0	37.5,[b] 35.84 ± 0.04,[c] 36[d]	78.3,[b] 78.36 ± 0.06,[c] 78[d]
	ϵ_1		5.2 ± 0.1[p]
	ϵ_∞	3.51 ± 0.08,[c] 2.5[d]	5.16 ± 0.14,[c] 4.5,[d] 3.3 ± 0.3[p]
Debye times	τ_{D1}, 10^{-12} s	3.506 ± 0.114[d]	8.5 ± 0.4,[p] 8.794 ± 0.595 [d]
	τ_{D2}, 10^{-12} s	0.177 ± 0.018[d]	0.170 ± 0.040,[p] 0.212 ± 0.055[d]
polarizabilities	α_{xx}, 10^{-24} cm^3	3.65,[f] *3.75*[g]	*1.468 ± 0.003*,[k] *1.495*[l]
	α_{yy}, 10^{-24} cm^3	3.65,[f] *3.75*[g]	*1.415 ± 0.013*,[k] *1.626*[l]
	α_{zz}, 10^{-24} cm^3	5.80,[f] *6.03*[g]	*1.528 ± 0.013*,[k]*1.286*[l]
mean polarizability	$\bar{\alpha}$, 10^{-24} cm^3	4.37,[f] *4.51*,[g] 4.325[c]	*1.470 ± 0.010*,[k] *1.469*,[l] 1.444 [c]
polarizability anisotropy	$\Delta\alpha$, 10^{-24} cm^3	2.15,[f]*2.28* [g]	*0.098*,[k] *0.297* [l]
relative 2nd hyperpolarizability	γ/γ_{N_2}	*4.41 ± 0.58*[i]	*1.87 ± 0.17*[i]

[a] $\bar{\alpha}$ and $\Delta\alpha$ are the mean and the anisotropy of the dipole polarizability, respectively, $\bar{\alpha} = (\alpha_{xx} + \alpha_{yy} + \alpha_{zz})/3$, $\Delta\alpha = (1/2)^{1/2}[(\alpha_{xx} - \alpha_{yy})^2 + (\alpha_{yy} - \alpha_{zz})^2 + (\alpha_{zz} - \alpha_{xx})^2]^{1/2}$. The dielectric dispersion is $\hat{\epsilon}(\omega) = (\epsilon_0 - \epsilon_1)/(1 + i\omega\tau_{D1}) + (\epsilon_1 - \epsilon_\infty)/(1 + i\omega\tau_{D2}) + \epsilon_\infty$. [b] Reference 57. [c] Reference 58. [d] Reference 59. [e] Reference 60. [f] Reference 61. [g] Reference 62. [h] Reference 63. [i] Reference 64. [j] Reference 65. [k] Reference 66. [l] Reference 67. [m] Reference 68. [n] Reference 69 for $x_{ACN} = 0.005$ at 25 °C. [o] Reference 70. [p] Reference 71.

femtolaser) serves as probe while the transmitted part is used for pumping. The pump beam passes a fast scanning device which consists of a triple mirror (PLX, OW-05−5) on an electromagnetic shaker (Brüel & Kjæ, 4810) driven by a frequency generator (Toellner, 7741) to an amplitude of ±0.5 mm at 72 Hz. A $\lambda/2$ plate (zero order; all crystal optics from Halle) and polarizer are set to produce linear electrical polarization of the pump field tilted by 45° from vertical. The probe beam is routed through a compensation delay (Physik Instrumente, M-150.11) which may be moved to desired positions for calibration (see below) with ±0.06 μm accuracy. Its polarization is rotated to vertical by a $\lambda/2$ plate, after which the beam enters the setup for measuring transient birefringence. This consists of a polarizer set for vertical (x) polarization, a $\lambda/4$ plate with its fast axis also vertical, and an analyzer which passes horizontally (y) polarized light only. The extinction ratio of the Glan-Thompson pair exceeds 10^6. For the sample cell we select a cuvette made of fused quartz with a 1-mm internal path length (Hellma). The cell is placed in a 1:1 telescope, with thin fused-quartz lenses of $f = 60$ mm, at optimal overlap of the pump and probe beams. The diameters of the beams are ≈3 mm (for 86% power transmission) on the first lens and their centers are spaced 6 mm apart. For Gaussian beams, their overlap in the propagation direction (z) should then be approximately Gaussian with fwhm 240 μm[88] well inside the liquid volume and below the collimation range.

Rotation of the polarizor around z by a small angle θ away from perfect crossing admits a local oscillator field E_{lo} out of phase with the signal field so that a dominant heterodyne transient signal $\boldsymbol{E}^*_{lo}\boldsymbol{E}_{signal} \propto \mathrm{Im}(\boldsymbol{\chi}_{eff})\theta$ records the induced optical birefringence. The homodyne contribution is eliminated by measuring kinetic traces for $\theta = \pm 1.8°$ and forming their difference.[74]

The interaction region in the sample is imaged to a plane ca. 3 m away, where an aperture discriminates against stray light from the cuvette windows. The transmitted light is detected with a cooled photomultiplier (Hamamatsu R6060). The signal current passing through a 0.3−100 kHz band filter is amplified (Stanford Research 570), sampled at 2 MHz, and A/D converted to 14-bit (GWU AIX). Typically 10^4 scans are summed. Because the shaker position has a cosine temporal dependence, a calibration of the time base is needed. This is done by recording OKE traces for several delay settings of the calibration stage, with pure water as sample. In this case the response is predominantly electronic and therefore instantaneous. For each setting, the coincidence of pump and probe pulses corresponds to a point along the shaker oscillation which is marked by a spike due to the electronic response. About 10−13 such measurements suffice to relate the sampling points to the true delay time.

Acetonitrile (Merck Uvasol) was used as received. Water was cleaned by ion exchange (Elgastat UHQ PS). The liquids were placed into the cuvette with a syringe equipped with a microfilter (0.2 μm, Sartorius RC15) and measurements were carried out at 21 ± 0.5 °C.

Results

Water: Simultaneous Determination of Pulse Shape and Spectral Density. The heterodyne Kerr trace $T(t)$ of the polarizability anisotropy Π_{xy} of water (normalized to its peak) is shown in Figure 2. The dynamic range of the induced birefringence extends over more than 4 decades and noise-equivalent power is reached at 1300 cm^{-1} in these measurements. The measured trace is given by the convolution[74]

$$T(t) = \int_{-\infty}^{+\infty} G(t')\, R(t - t')\mathrm{d}t' \qquad (1)$$

Here $G(t)$ is the pump−probe intensity correlation function and the system response $R(t)$ consists of an electronic part which is instantaneous (delta function) and a time-dependent nuclear part:

$$R(t) = R_{el}\delta(t) + R_{nuc}(t) \qquad (2)$$

To obtain the spectral density $\chi(\omega)$ of the response (see Appendix A) from the time-dependent birefringence, the "effective pulse" $G(t)$ is needed for deconvolution and is usually measured by second harmonic generation (SHG). For pump and probe fields which are identical (apart for an amplitude factor), this function is symmetrical in time. However, the pump and probe beams may not be completely equivalent for very short (∼10 fs) pulses so that some deviation of $G(t)$ from symmetry is to be expected. Here we describe how the correct intensity correlation function can be determined from a time-resolved OKE measurement of materials with low nuclear response such as water. (Of course SHG at the exact interaction position or

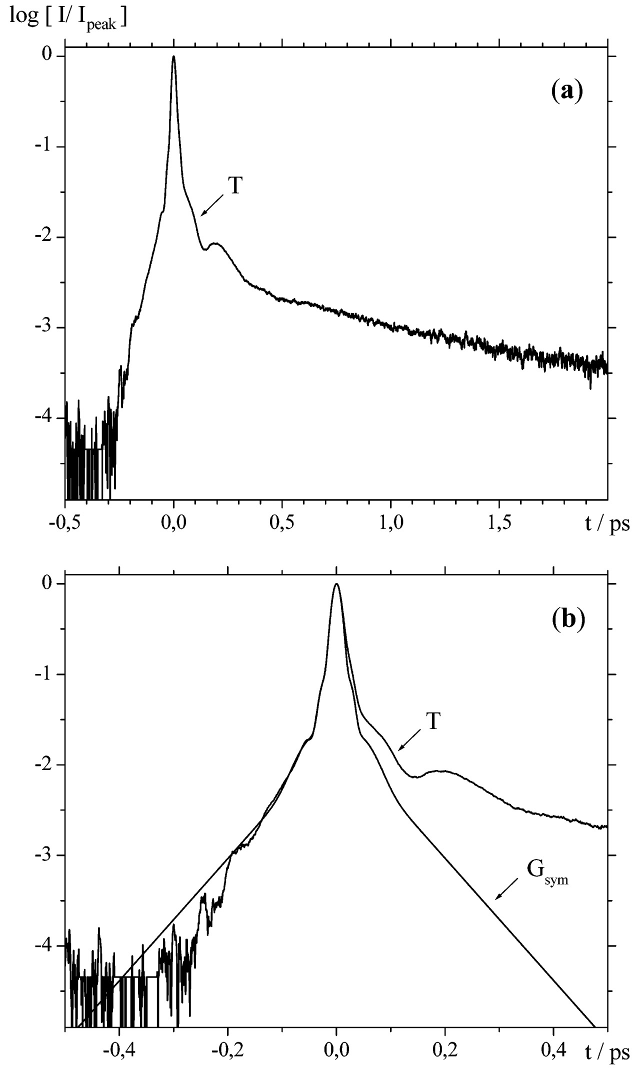

Figure 2. Heterodyne optical birefringence trace T of water and the symmetrical effective pulse G_{sym}, which was derived from the rising part of T.

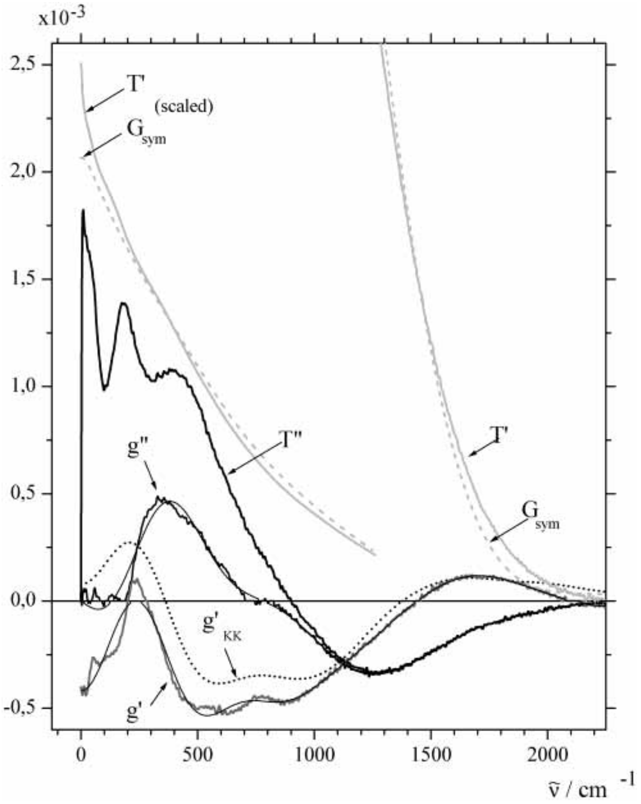

Figure 3. Fourier transforms $T' + iT''$ of the birefringence trace and G_{sym} of the symmetrical pulse in Figure 2. Values for T' and G_{sym} extend over a large range and are therefore shown scaled (by a factor of 1/13) for $\tilde{\nu} \leq 1250$ cm^{-1}. Negative T'' at high frequencies indicates an asymmetrical contribution G_{asym} to the effective pulse, which is estimated initially as $g' + ig''$ (see text). g'_{KK} was constructed from g'' by the Kramers−Kronig relation.

its equilvalent would also provide $G(t)$, but this is both inconvenient and more susceptible to systematic errors because of bandwidth limitations.)

The initial part of the water OKE signal up to its peak and just beyond (cf. Figure 2b) can be assigned to electronic response only and therefore is taken for the intensity correlation function there. In a first approximation, the latter is modeled with a *symmetric* function $G_{sym}(t)$ and the corresponding parameters are found by data fitting. For a model function we need a central Gaussian which is flanked, symmetrically on either side, by two Gaussian shoulders on an exponential pedestal. The peak position of the fitted pulse model, which need not coincide with a time data point, is taken to indicate time zero. Next the tail of the OKE trace is fitted by an exponential and thereby extended for Fourier transformation. In the frequency domain, then, the transformed symmetric function and the transformed water trace are both time-shifted such that correct time zero applies; the resulting $G_{sym}(\omega)$, $T'(\omega)$, and $T''(\omega)$ are shown in Figure 3. If the pulse was indeed symmetrical then deconvolution T''/G_{sym} by the pulse spectrum should give the spectral density.[89] It is readily seen from Figure 3 that the nuclear spectral density χ_{nuc} is thus predicted to be strongly negative at all frequencies above 1000 cm^{-1} which is unphysical. Usually the measured trace is time-shifted to $T(t - \Delta t)$ in order to compensate. But in the present case, $\Delta t = -0.7$ fs would be required, which is much larger than the uncertainty in determining time zero and therefore is not allowed. Instead we conclude that the symmetrical time function for the effective pulse is not adequate for deconvolution and should be augmented:

$$G(t) = G_{\mathrm{sym}}(t) + G_{\mathrm{asym}}(t). \tag{3}$$

Note that the last term is small (compare Figure 2b and Figure 5a) and vanishes for t ≤ 0 since the symmetric term was already fitted to the trace there. On the other hand, at frequencies well below the spectral pulse width we may indeed approximate

$$\chi''_{\mathrm{nuc}}(\omega) \approx T''(\omega)/G_{\mathrm{sym}}(\omega) \tag{4}$$

which is shown in Figure 4 (thick solid line).

Now the crucial step in the procedure is to adopt a model for water nuclear susceptibility (constructed from line shape functions, Appendix A) which is flexible at low frequencies and which also contains high-frequency modes transferred from depolarized Raman spectra. For a start we take the multimode Brownian oscillator (BO) model of Palese et al.[80] who included Rayleigh scattering data from Walrafen;[79] this is shown as a dashed line χ_a'' in Figure 4. Modification and fitting to our χ''_{nuc} below 200 cm^{-1} (while keeping the high-frequency part) gives an improved model χ_b, the spectral density of which is also shown in the figure.

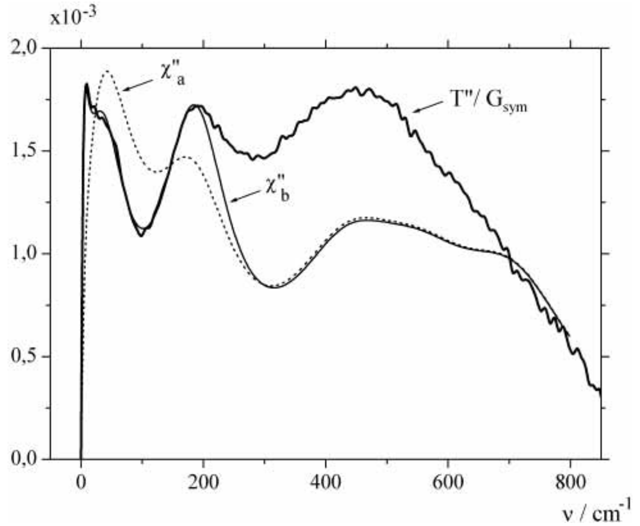

Figure 4. Estimate of the nuclear spectral density χ''_{nuc} of water at low frequencies from our measurements, T''/G_{sym}, and multimode Brownian oscillator models χ''_{a} (ref 80) and χ''_{b} with modes >400 cm^{-1} transferred from depolarized Rayleigh spectroscopy (ref 79) (see text).

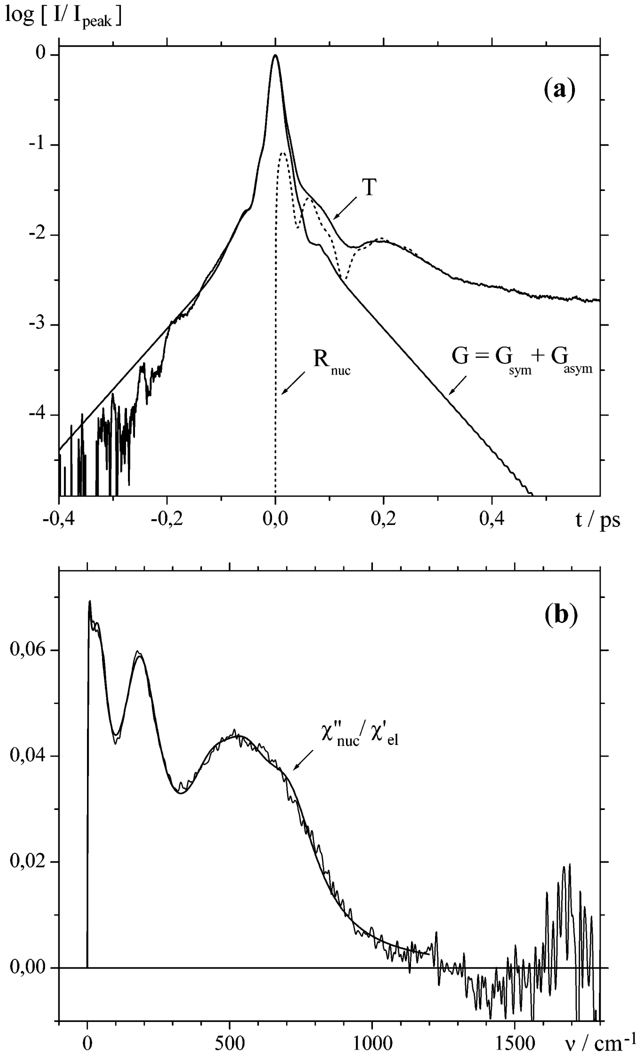

Figure 5. (a) Heterodyne optical birefringence trace T of water, the effective pulse G, and the deconvoluted nuclear response R_{nuc} of water. **(b)** Deconvoluted spectral density for the polarizability anisotropy of water at 294 K, relative to the electronic susceptibility of water.

TABLE 2: Parameters for OKE Spectral Density (Eq A6) and Friction Relaxation (Eq A8)[a]

	$\omega_0/2\pi c$, cm^{-1}	$\gamma/2\pi c$, cm^{-1}	τ_F, ps	amplitude
water $\chi(\omega)$ (Figures 5b, 8, 12b)	21.26	70.81	0	0.107
	58.69	86.75	0	0.0518
	204.4	188.61	0	0.0437
	450	250	0	0.0114
	570	250	0	0.009 48
	720	250	0	0.007 53
composite $\chi(\omega)$ (Figure 12b)	8.81	48.63	0	16.909
	32.68	52.29	0.0559	3.709
	78.85	80.16	0.0181	2.187
acetonitrile $\chi(\omega)$ (Figure 12b)	11.89	43.95	0	10.55
	35.11	59.00	0.0571	4.503
	81.09	78.05	0.0179	1.730
dilute acetonitrile $\chi(\omega)$ (Figure 11a)	6.94	21.14	0	10.941
	34.74	63.86	0.0571	6.053
	86.92	74.82	0.0182	1.307
friction relaxation $\xi(t)$ (Figure 11b)	17.9 ± 0.4	53.6 ± 2.1	0	34.2 ± 0.9
	43.7 ± 1.2	72.2 ± 3.9	0	33.9 ± 1.6
	106.4 ± 3.0	110.6 ± 7.0	0	45.0 ± 6.3
	3917 ± 31	62407 ± 1600	0	538 ± 14

[a] More digits are given than is significant to allow reproduction of figures.

To determine the correlation function one needs to find the asymmetric correction $G_{\text{asym}}(t)$. Let us return to the frequency domain and observe that

$$G(\omega) = T(\omega)/(\chi_{\text{nuc}}(\omega) + \chi_{\text{el}}) \tag{5}$$

and

$$G_{\text{asym}}(\omega) = T(\omega)/(\chi_{\text{nuc}}(\omega) + \chi_{el}) - G_{\text{sym}}(\omega) \tag{6}$$

the real and imaginary parts of which must be related by the Kramers–Kronig relation[34] since $G_{\text{asym}}(t) \equiv 0$ for $t \leq 0$ by definition. The procedure therefore is as follows. First assume some (real) trial value χ for the electronic susceptibility in eq 6, approximate the nuclear susceptibility by $\chi_b(\omega)$, and calculate the spectrum of the trial asymmetric term

$$g(\omega) = T(\omega)/(\chi_{\text{b}}(\omega) + \chi) - G_{\text{sym}}(\omega) \tag{7}$$

In Figure 3 we show g' and g'', which are obtained when the total area under the symmetric pulse $G_{\text{sym}}(t)$ is used for χ. For convenience the real and imaginary parts of g are then expanded into orthogonal Hermitian polynomials which are derived from the central Gaussian in $G_{\text{sym}}(\omega)$. From this analytical representation of g'', for example, the corresponding real part g'_{KK} is calculated with the Kramers–Kronig relation. In Figure 3 it is readily seen that g'_{KK} (dashed line) has a shape which is similar to that of g' but that the two spectral functions still differ significantly. Remember that they should be identical if the true electronic and nuclear susceptibilities are used—this suggests that our trial χ and $\chi_{\text{b}}(\omega)$ be varied such that the deviations $g'(\omega) - g'_{\text{KK}}(\omega)$are minimized. In that case we have $g \equiv G_{\text{asym}}(\omega)$ and inverse Laplace transformation gives $G_{\text{asym}}(t)$. The result for water is summarized in Figure 5. The bottom panel shows the nuclear susceptibility $\chi''_{\text{nuc}}(\omega)$ deconvoluted from our OKE measurement together with its model description (smooth line, parameters in Table 2). The latter is presented relative to the water electronic susceptibility χ_{el}, which is adopted as reference throughout this paper. The top panel shows again the normalized Kerr trace of water. Now this is underlaid by the effective pulse $G(t)$ and by the nuclear response function $R(t)$, which is obtained from $\chi''_{\text{nuc}}(\omega)$ with the help of the

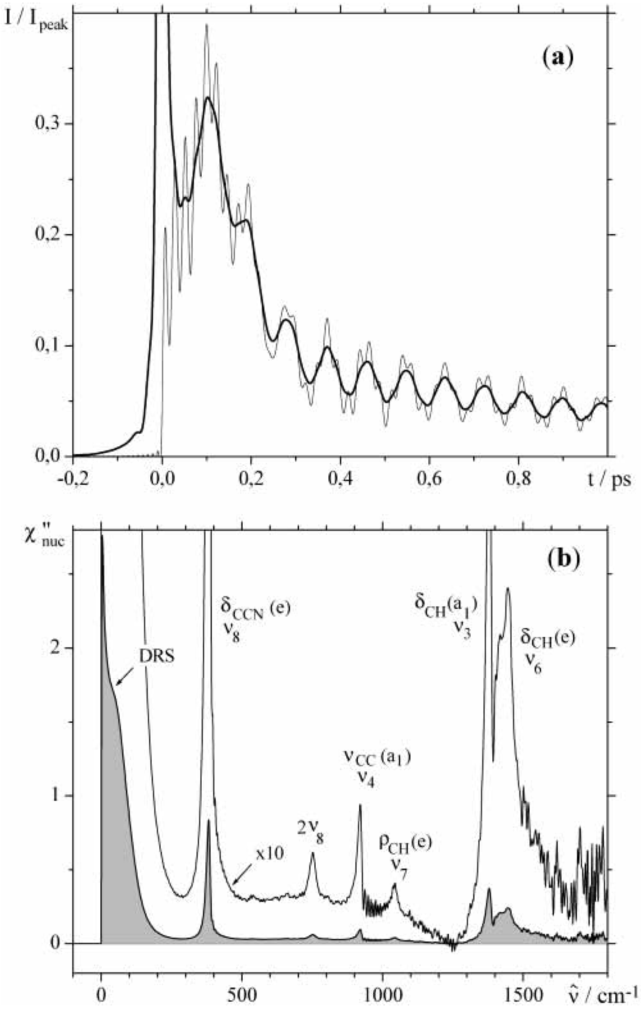

Figure 6. (a) Heterodyne optical birefringence trace of acetonitrile (thick line) and the deconvoluted nuclear response (thin line). **(b)** OKE spectral density of acetonitrile at 294 K, relative to the electronic susceptibility of acetonitrile, with assignments for Raman bands. Only depolarized Rayleigh scattering (DRS) will be considered here (The line is the same as the shaded part, only multiplied by 10).

fluctuation−dissipation theorem assuming linear response, as outlined by Lotshaw et al.[74]

The utility of our deconvolution technique becomes apparent when the pulse shape derived here is employed in subsequent measurements, such as of pure acetonitrile, which will be examined next.

Acetonitrile: Improved DRS Spectrum. The heterodyne OKE trace of pure acetonitrile (ACN) is shown in Figure 6a (thick solid line) and the corresponding nuclear susceptibility is presented in Figure 6b. When the effective pulse is transferred from the previous measurement with water, its time shift relative to the peak of the ACN trace remains the only free parameter. After deconvolution the shift was adjusted such that the spectral density becomes zero around 1250 cm^{-1}—equivalent to assuming that collision-induced processes have this effective upper frequency limit (note that general theory[10] predicts an ohmic line shape so that the spectral density may be made arbitrarily small by going to high enough frequencies). Intramolecular vibrational modes which are known from depolarized Raman spectroscopy[65,90,91] are observed up to 1500 cm^{-1} in Figure 6b.[92] To illustrate the possibilities of high signal/noise together with adequate data treatment, we backtransform[74] and show in Figure 6a the complete nuclear response (thin line) superimposed onto the measured trace.

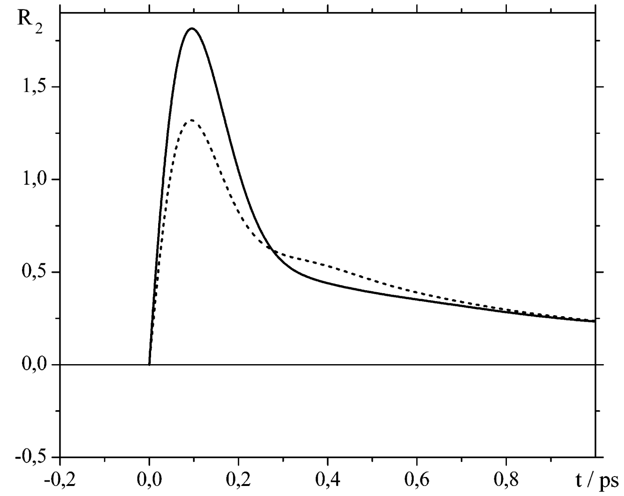

Figure 7. Normalized polarizability anisotropy response of pure acetonitrile (solid line, from DRS band of Figure 6b) and equivalent response obtained from $\epsilon(\omega)$ (dashed line, see text).

Depolarized Rayleigh scattering (DRS) below the degenerate CCN bending vibration was empirically fitted by Mori line shape functions (Appendix A) and the parameters are given in Table 2. Its backtransform[74] gives the collective intermolecular Π_{xy} response $R_2(t)$, which (normalized to its time integral) is shown as solid line in Figure 7. Our result qualitatively reproduces earlier reports,[93−95] but we find a somewhat smaller contribution of the high-frequency, nondiffusive part. The diffusive limit appears to be reached by 1 ps. In this case the polarizability and transverse polarization response functions may be related by a power law between their underlying rank 2 and rank 1 correlation functions, respectively.[96] The latter is constructed from the susceptibility for transverse polarization which was obtained[97] by combining far-infrared[98] and microwave[99] data. By invoking the power law and then forming the time derivative, the dashed line in Figure 7 is produced (in addition, the amplitude was adjusted so that the Π_{xy} response is followed beyond 1 ps.) After the initial peak, a second "hump" around 0.4 ps indicates the fact that collective *dipole* relaxation of liquid acetonitrile is slightly underdamped.[97,100−104] Returning to the polarizability response, it exhibits no such underdamped behavior in bulk acetonitrile. But we will show later that an oscillation of the polarizability anisotropy emerges if acetonitrile is diluted in water.

Finally for this section, the electronic response of water and acetonitrile was also compared in successive OKE measurements followed by deconvolution: we find $\chi'^{(\mathrm{acetonitrile})}_{\mathrm{el}}/\chi'^{(\mathrm{water})}_{\mathrm{el}} = 2.66$ for the ratio of the molar response at 795 nm. This may be compared with a ratio 2.36 ± 0.38 of dynamic second-order hyperpolarizibilities from EFISH measurements at 1064 nm.[64]

Acetonitrile/Water Mixtures: Analysis by Mole-Fraction Weighted Data Fitting. Time-resolved OKE measurements were then performed for acetonitrile/water mixtures for several acetonitrile mole fractions x_{ACN}. We are primarily interested in the low-frequency region ≤ 300 cm^{-1}, which is dominated by Rayleigh scattering due to intermolecular (librational and translational) modes. Contributions to the spectral density coming from the strong intramolecular CCN bending mode are (approximately) removed by fitting the latter with a Brownian oscillator line shape (eq A2) and subtraction of the fit from the data. Next the various susceptibility spectra must be placed on a common ordinate scale. We take the molar electronic response of water for reference and assume that the electronic response of a mixture is ideal, i.e., made up from the molar response of

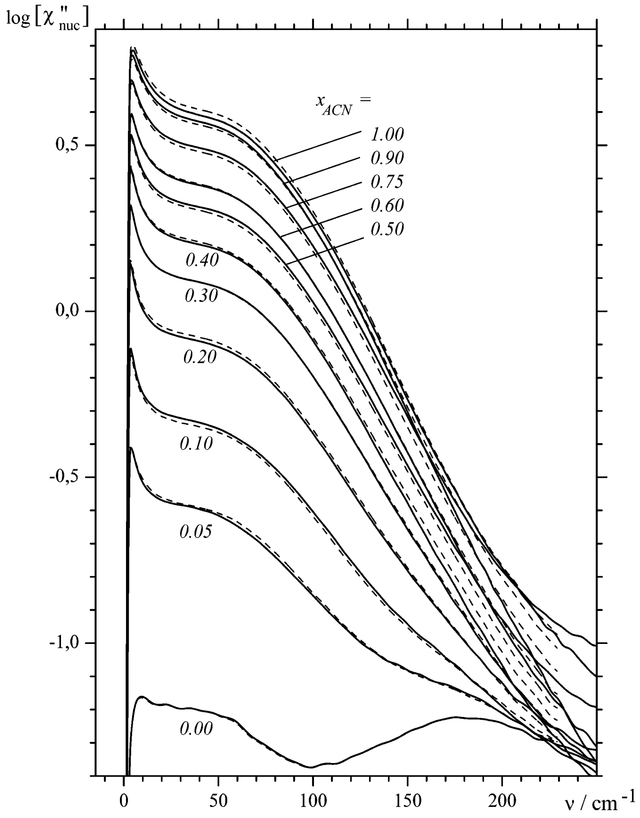

Figure 8. DRS spectral density of acetonitrile/water mixtures depending on acetonitrile mole fraction (solid lines), relative to the electronic susceptibility of pure water. Interpolations from the global model in Figure 11 are also indicated (dashed lines).

the components according to composition. In this way effects due to volume changes upon mixing are taken into account implicitly.[59,105] All $\chi(\omega)$ from now on should be understood as so referenced and are therefore dimensionless. Linearity of the amplitude for the bending mode could also have been used for scaling but is less accurate.

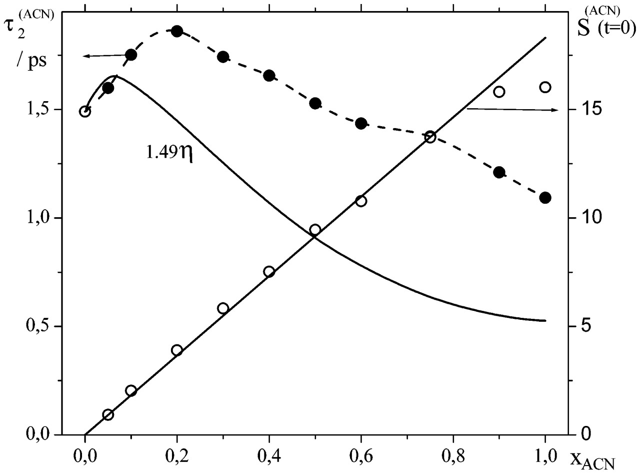

Figure 9. Correlation times $\tau_2^{(ACN)}$ (solid circles, connected for better viewing only) and DRS band integral $S^{(ACN)}(t = 0)$ (empty circles) due to the acetonitrile solute, i.e., after subtraction of the ideal water contribution, depending on mole fraction. The band integral which is expected for noninteracting solutes is indicated with a solid line. The viscosity (scaled to the correlation time at infinite dilution) is given for comparison.

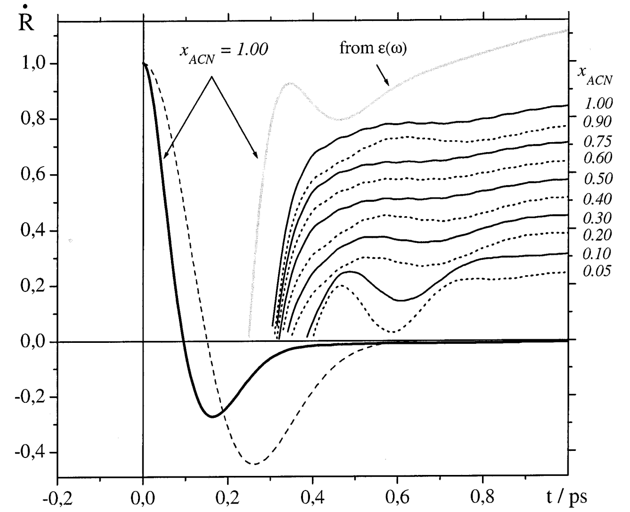

Figure 10. Velocity correlation functions for polarizability anisotropy, fully shown for pure acetonitrile (thick solid line) but limited to $t > 0.3$ for other mole fractions (magnified x15 and offset). An equivalent function derived from $\epsilon(\omega)$ is also shown (magnified x15 and offset; gray line). The long-dashed line is derived from the initial, but continued, Gaussian relaxation for comparison. A librational oscillation in pure acetonitrile is visible with far-IR but not with DRS spectroscopy. For dilute acetonitrile in water a librational oscillation is again observed, but with lower frequency because of a different surrounding.

The DRS spectra which are obtained in this way are shown in Figure 8 on a semilogarithmic scale. They are dominated by acetonitrile as its mole fraction x_{ACN} is increased because of the low polarizability anisotropy of water, as can be seen from Table 1. Apart from increasing amplitude, however, there appears to be only minor change in the spectra. In particular near the critical composition $x_{\mathrm{can}} = 0.364$[106] there is no obvious indication of the demixing point below, at 271.9 K. However, it should be noted that the nature of the observable changes as one moves from dilute aqueous acetonitrile, single and with small collisional interaction, to neat acetonitrile, with collective response and strong collisional contribution.[107] Therefore opposite trends may cancel and small spectral change does not imply that the dynamics remains nearly identical across the compositional range. Later we shall expose spectral change by mole-fraction weighted data fitting. But first let us look at each $\chi''_{\mathrm{nuc}}(\omega,x_{\mathrm{ACN}})$ individually, by determining spectral parameters which are then compared. If the weighted water spectrum $(1 - x_{\mathrm{ACN}})\chi''^{(\mathrm{water})}_{\mathrm{nuc}}(\omega)$[108] is subtracted, then an excess part $\chi''^{(\mathrm{ACN})}_{\mathrm{nuc}}(\omega,x_{\mathrm{ACN}})$ is obtained: it should approximate the signal from acetonitrile only. (For this and the next paragraph we now drop the mole fraction in the notation). The corresponding relaxation function $S^{(\mathrm{ACN})}(t)$ is then constructed from the excess spectral density data. It refers to the collective polarizability anisotropy Π_{xy} caused by acetonitrile and $S^{(\mathrm{ACN})}(t = 0) \equiv \int_0^\infty \chi''^{(\mathrm{ACN})}(\omega)\,\mathrm{d}\omega$ gauges the optical coupling strength in one mole of the mixture. The rank 2 correlation time is given by

$$\tau_2^{(ACN)} = \int_0^\infty S^{(\mathrm{ACN})}(t)\,\mathrm{d}t/S^{(\mathrm{ACN})}(t = 0) \qquad (8)$$

These integral parameters are shown in Figure 9 depending on x_{ACN}.

High-frequency features are best discussed in terms of velocity correlation functions which are obtained by transformation of the $\omega\chi''^{(\mathrm{ACN})}_{\mathrm{nuc}}(\omega)$. These functions are discussed with the help of Figure 10 where the full solid line refers to pure ACN. An initial positive part reflects the impulsive creation of the birefringence, while a subsequent negative part corresponds to its decay. The velocity correlation functions for the mixtures are presented (magnified x15 and offset) only for $t > 0.3$ ps.

Upon dilution a weak oscillation emerges around $x_{ACN} \approx 0.50$, the frequency of which shifts upward as damping is relieved or correlation with neighboring solutes is removed. One may be concerned that the entire effect is created artificially by the subtraction of the water spectrum, which is justified at infinite dilution but possibly not at $x_{ACN} = 0.05$. However, in the latter case the oscillation persists even if the full spectral density is employed, while pure water shows no effect. Furthermore the frequency resembles that of dipolar librations in pure acetonitrile, which was already mentioned. To see this we also show the hypothetical second-rank velocity correlation function which was constructed from $\epsilon(\omega)$ (i.e., time derivative of the dashed line in Figure 7). We conclude that dilute acetonitrile in water performs librational oscillations which are observable by DRS or time-resolved OKE measurements and note that the known librations in pure acetonitrile[97,100−104] are not observed in this way. The composition dependence of the spectra in Figure 8 is needed for extrapolation but is interesting by itself, in view of the proposed (and controversial) microheterogenity of the acetonitrile/water system.[78] It may be analyzed, for example, by describing each spectrum in terms of line shape functions and noting their parameters as $x_{ACN} \equiv x$ is increased. The various bands may then be associated with processes such as rotational diffusion,[2] librational motion, or collisional interaction.[63,81−87,102,107] We follow a more empirical approach and expand $\chi''_{nuc}(\omega,x)$, in the least-squares sense, into linearly independent functions of x. Mole-weighted fitting has been used for terahertz infrared spectra of acetonitrile/CCl_4 mixtures.[109] Here we employ target singular-value decomposition (SVD)[110] for this purpose. The spectral integral ranges decreases over 2 decades with acetonitrile dilution, at the end of which the water spectrum must be represented well: both aspects require a modification which is presented in Appendix B. The analysis is restricted to frequencies below 230 cm^{-1} in order to minimize collisional background, which (at least for dilute solutions) may be presumed to have ohmic band shape.[10]

We find that a basis set of only three spectra allows to describe every $\chi''_{nuc}(\omega,x)$ with expansion coefficients $\{v_k(x)\}_{k=1,3}$ to within noise. However, this description is completely empirical and for physical insight we must introduce compositional or weight functions $T_j(x)$.[111] For example a first function $(1 - x)$ would represent bulk water, a second function x^1 would represent acetonitrile monomers, and x^2, ..., x^6 would stand for dimers up to hexamers provided the dynamics were inhomogeneous. The empirical coefficients $v_k(x)$ are then fitted by these model functions and each $T_j(x)$ generates an "species associated spectrum" $\chi''^{(j)}(\omega)$ (SAS—note that some of these may be linearly dependent). In our case a perfect description, that is down to noise for each measured spectrum in Figure 7, requires the power series

$$\chi''_{nuc}(\omega,x) = (1 - x)\chi''^{(water)}_{nuc}(\omega) + x\chi''^{(1)}(\omega) + ... + x^6\chi''^{(6)}(\omega) \quad (9)$$

Here the nuclear spectral density $\chi''^{(water)}_{nuc}$ of bulk water is known already. The spectral density for single acetonitrile molecules surrounded by water is given by $\chi''^{(1)}(\omega)$; it is shown in Figure 11a and presented in Table 2 in terms of Mori line shape functions (Appendix A).

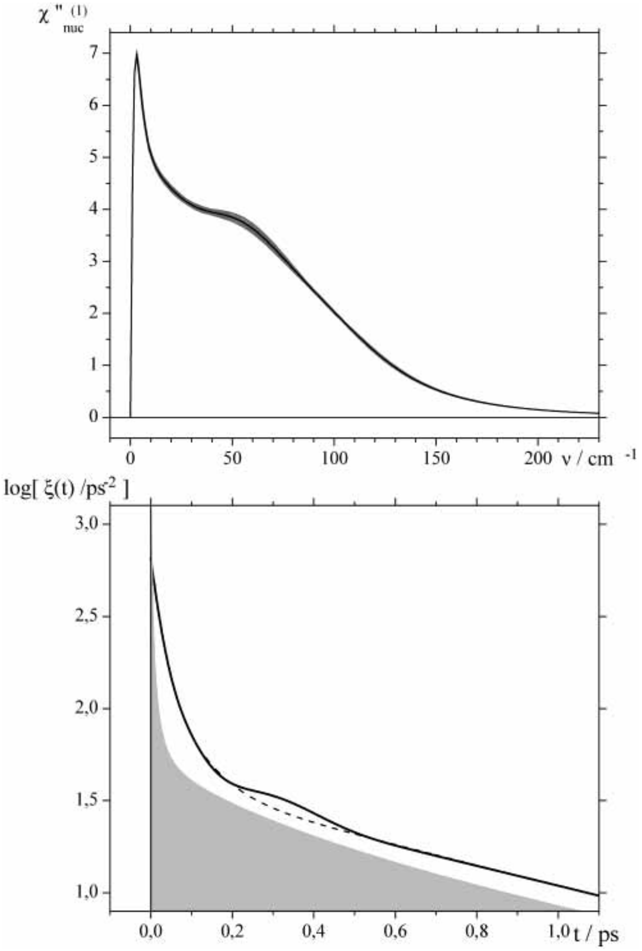

Figure 11. (**a**) Spectral component $\chi''^{(1)}(\omega)$ associated with acetonitrile mole fraction x_{ACN} (dots) and description with a single line shape function (black solid line) involving frequency-dependent friction. Spectra which are produced when parameters are varied (see text) are given by gray lines. (**b**) Rotational friction kernel $\xi_2(t)$ underlying the spectrum in the upper panel (solid line) and approximate description by exponentials (dashed line). The shaded part represents the kernel from dielectric theory with $y = 0.3$ (see text).

In the cluster model used so far, many virtual "species" and associated spectra were considered. The question arises if a simpler model can be found which nonetheless captures the essence of the compositional dependence of the depolarized Rayleigh spectra. We intend to use the spectrum of pure water, that of pure acetonitrile, and a third spectrum which will be taken to refer to a "composite species". The latter spectrum is to be determined together with the relative weights of the three "species". For water, again ideal behavior is prescribed: $T_{water}(x) = 1 - x$. Deviation from ideality will thus be embodied in the other compositional weights and in the composite spectrum. The remaining ACN mole fraction must now be partitioned: $x = T_{ACN}(x) + T_{comp}(x)$, so that one only needs to find a reasonable form for the weight $T_{comp}(x)$ of the composite species. An initial guess $(1 - x)x$ was improved to $T_{comp}(x) = (1 - x)^{\alpha}x^{\beta}$ by inspection and optimization gave parameters $\alpha = 1.23$, $\beta = 1.19$. The result is summarized in Figure 12. The upper panel shows the weights of the three species as function of x. Remember that the molecular polarizability anisotropy of H_2O is orders of magnitude below that of CH_3CN, so that the signal due to water becomes insignificant from some ACN mole fraction onward. This can be seen in the upper panel: the water weights, as determined by SVD, scatter wildly from the prescribed line for $x > 0.30$. The lower panel shows the three species-associated spectra, of which $\chi^{(comp)}$ is new, while the others refer to pure water and pure acetonitrile. Note that the "composite spectrum" alone does *not* represent acetonitrile in the limit of infinite dilution. This is because the slopes of both $T_{ACN}(x)$ and $T_{comp}(x)$ are similar as $x \to 0$ so that both $\chi''^{(ACN)}$

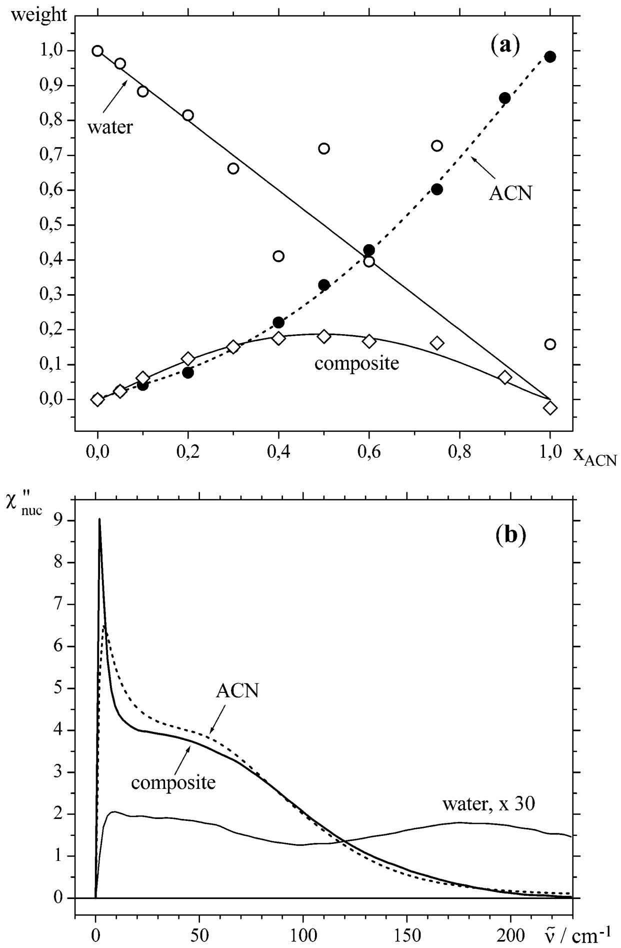

Figure 12. Behavior of the DRS spectra in Figure 8 with acetonitrile mole fraction. The spectra are decomposed into the water spectrum which declines as $1 - x_{ACN}$, the acetonitrile spectrum, and a "composite" spectrum. The parameters for the basic spectra are collected in Table 2.

and $\chi''^{(comp)}$ contribute. In comparison with the polynomial expansion above, we find $\chi''^{(1)} \approx 0.595\chi''^{(ACN)} + 0.804\chi''^{(comp)}$. To represent and handle these spectra, they were fitted with Mori line shape functions (eq A6) and the parameters are also listed in Table 2. In Figure 8, each measured spectrum can now be compared with its simulated counterpart (dashed lines). (The Mori fits are by no means unique; for example, several Brownian oscillator line shapes would also describe the spectra. Such fits are only used for an empirical representation and the corresponding parameters will not be interpreted.)

Discussion

Dilute Acetonitrile in Water: Determination of the Friction Kernel from the DRS Line Shape. We begin the discussion with dilute acetonitrile as molecular Raman probe in water. The corresponding DRS spectrum was already shown in Figure 11a and constitutes the main experimental result of this work. In fact at the lowest acetonitrile mole fraction measured, on average only 2.7 water molecules in each direction separate the acetonitriles and orientational correlations between the latter are therefore expected. On the other hand, extrapolation of the measured spectra to infinite dilution should have reduced correlational features further, at least qualitatively. With this understanding of the experimental situation, the spectrum in Figure 11a will be treated as that of single acetonitrile molecules infinitely surrounded by water, and possible deviations will be examined afterward.

Dilute acetonitrile ($x_{ACN} < 0.05$) has slightly negative excess volume of mixing in water and the enthalpy of mixing is negative.[112] This suggests that CH_3CN occupies a "cavity" in the water structure where it is H-bonded through the nitrogen atom.[78] H-bonding is supported by analysis of the CN stretch contour (~2253 cm^{-1} for free CH_3CN and blue-shifted upon bonding to ~2258 cm^{-1}) from Raman and IR spectroscopy of acetonitrile−water mixtures.[57,113] From IR data it was inferred that 10% of the CH_3CN molecules are not hydrogen bonded for $x_{ACN} \approx 0.05$ and that −O−H---N bonds decrease faster upon further dilution than −O−H---O bonds are created.[113] However, Monte Carlo simulations modeling the hydration of the sp nitrogen showed approximately 1.3−1.4 water molecules around the nitrogen atom in the first shell all of which are hydrogen bonded, while no hydrogen bonds were found in the methyl region, which is hydrated by 19 water molecules in the first shell.[114]

Extending from the CH_3CN solute into the liquid, the water structure and dynamics is perturbed by the presence of the organic component. This is reflected in the variation of the ACN rotational diffusion time from NMR[55] with composition even below $x_{ACN} \approx 0.02$. A major difference between H_2O and CH_3CN is that the former acts both as acceptor and donor of two hydrogen bonds, while the latter can only accept one hydrogen bond. This leads to a discontinuity in the three-dimensional water network, which is disrupted when CH_3CN is incorporated into the structure, and the change is enhanced by the hydrophobic interaction between the methyl group and the neighboring polar water molecules. Thus acetonitrile may act rather like small ions that partially melt the H-bonded water structure.[115]

A microscopic picture thus emerges of single CH_3CN molecules which are likely to be H-bonded through the nitrogen atom, have repulsive (hydrophobic) interactions to their surrounding elsewhere, and induce structural change in the water H-bonded network further away. Since the mean polarizability $\bar{\alpha}$ of CH_3CN is at least 4 times larger than that of H_2O (Table 1), collisional effects between the two can safely be neglected. Remember that when extrapolating the DRS spectra, the ideal contribution of pure water was already subtracted so that the spectrum should reflect CH_3CN orientational dynamics only. Taken together it seems reasonable to assume the homogeneous limit and describe the DRS spectrum of Figure 11a with a single line shape based on frequency-dependent friction. The line shape function will be presented next, following closely the work by Madden and Kivelson.[18]

The optical Kerr response is related to an off-diagonal component, Π_{xy}, of the collective polarizability Π. Actually, all signals were referenced to the molar electronic susceptibility $\chi_{el}^{(water)}(\omega) = N_A\gamma_{el}^{(water)}$ of water when constructing the spectra in Figure 8. Neglecting collision-induced effects, we therefore have for the (dimensionless) signal relaxation

$$S^{(ACN)}(t) \equiv \frac{\langle \Pi_{xy}(0)\,\Pi_{xy}(t)\rangle}{N_A\gamma_{el}^{(water)}} = \frac{1}{15}\frac{N\Delta\alpha^2}{N_A\gamma_{el}^{(water)}}\sum_{j}^{N}\langle P_2[\vec{\Omega}_1(0)\cdot\vec{\Omega}_j(t)]\rangle \quad (10)$$

and the corresponding rank 2 relaxation function

$$C_2(t) = S^{(ACN)}(t)/S^{(ACN)}(t = 0) \quad (11)$$

Here $\vec{\Omega}_j$ is the unit vector pointing along the symmetry axis of acetonitrile molecule j in the sampled volume, $\langle\,\rangle$ denotes averaging over an equilibrium ensemble containing N acetonitrile molecules with polarizability anisotropy $\Delta\alpha = \alpha_7 - \alpha$ per mole of the mixture. P_2 is the second Legendre polynomial. For dilute acetonitrile the cross terms $1 \neq j$ can be neglected and the orientation $\vec{\Omega}$ for a representative single molecule (here: the first) remains. N_A is Avogadro's number and $\gamma_{el}^{(water)}$ the molecular second dynamic electronic hyperpolarizability of water. Remember that the notation $S^{(ACN)}(t)$ indicates signal from the dilute solute only since the ideal water contribution has been removed.

Generally an orientational correlation function of rank L is defined as

$$C_L(t) = \sum_j^N \langle P_L[\vec{\Omega}_1(0)\cdot\vec{\Omega}_j(t)]\rangle / \sum_j^N \langle P_L[\vec{\Omega}_1(0)\cdot\vec{\Omega}_j(0)]\rangle \quad (12)$$

$C_L(t)$ arises from a generalized Langevin equation for the angular velocity $\dot{\vec{\Omega}} \equiv \vec{\omega}$ of the type[116]

$$I_B\frac{d}{dt}\vec{\omega} + \int_0^\infty dt'\, I_B\xi(t')\vec{\omega}(t-t') = \vec{R}(t) \quad (13)$$

where I_B is the moment of inertia for tumbling motion. For a linear molecule the random torque $\vec{R}(t)$is related to the dynamic friction $\xi(t)$ (ps^{-2}) by

$$I_B\xi(t) = \frac{1}{2kT}\langle\vec{R}(0)\vec{R}(t)\rangle \quad (14)$$

with Boltzmann constant k and absolute temperature T. After Laplace transformation (Appendix A, $s = -i\omega$) a convenient approximation to an orientational correlation function is achieved by Mori's continued fraction,[13b] which is truncated to second order (in our case rank $L = 2$):

$$\hat{C}_L(s) = \cfrac{1}{s + \cfrac{K_L(0)}{s + \hat{\xi}_L(s)}} \quad (15)$$

$K_L(0)$ is the value for the pertinent velocity friction kernel at $t = 0$; for free rotation

$$K_L(0) = L(L+1)kT/I_B = \omega_{0L}^{\;2} \quad (16)$$

The Einstein frequency ω_{0L} governs the initial decay as

$$C_L(t) \approx 1 - \frac{1}{2}\omega_{0L}^{\;2}t^2 + ... \quad (17)$$

$\hat{\xi}_L(s)$ is the transform of the intermolecular dynamic force friction kernel $\xi_L(t)$, which was illustrated in Figure 1. The acetonitrile solute experiences a fluctuating torque from translational motion of nearby water molecules through short-range (SR) interactions. Solvent rotational motion, on the other hand, creates a fluctuating torque through dipole−dipole (DD) interactions. Madden and Kivelson[18a] assumed that both mechanisms can be separated and decomposed the frictional torque into a fast-relaxing SR part, taken to be delta-correlated, and into a slow-relaxing DD part, whose correlation decays multiexponentially. Kumar and Maroncelli[21] examined this hypothesis by molecular dynamics simulations of a simple polar solute in acetonitrile and methanol. They found that nearby solvent molecules are pulled up the repulsive wall of the solute by Coulomb interaction. As these solvent molecules rotate they also exert short-range forces onto the solute, which is why the two kinds of frictional mechanism are correlated and friction cannot be decomposed.

Returning to an acetonitrile solute surrounded by water, we intend to provide the friction function $\xi_2(t)$ from experiment so that it may be compared with theory or simulations. Inverting eq 15 one has

$$\hat{\xi}_L(s) = \frac{K_L(0)}{1/\hat{C}_L(s) - s} - s \quad (18)$$

with $L = 2$ for DRS. The relaxation spectrum $\hat{C}_2(s)$ is available through an empirical description of the DRS spectrum by Mori line shape functions (Appendix A with Table 2) and $K_2(0) = 26.72$ ps^{-2} or $\omega_{02}/2\pi c = 27.44$ cm^{-1} from the inertial moment (Table 1). When both sets of data are used in eq 18 then a component $-\rho s$ is generated in $\hat{\xi}_2(s)$ which is easily recognized and fitted to give $\rho = 0.222$. However, this contribution is unphysical in the context of friction and we see from eq 15 that it should be absorbed in the Einstein frequency squared, which now becomes $K_2(0)/(1 - \rho)$. The Einstein frequency is thus raised from a value for thermal free rotation to 31.11 cm^{-1} (as is best seen directly when fitting $C_2(t)$ at early times to eq 17). It is interesting to speculate on the reason for this increase. For example the moment of inertia I_B may be decreased through a contraction of the C−C and C=N bonds. Indeed upon solvation in water, a decrease of the C≡N bond length relative to the gas phase is indicated by IR and Raman spectroscopy,[57] but this effect is an order of magnitude below the total upshift of the Einstein frequency. Another reason may be that, contrary to our assumptions, neighboring acetonitrile solutes are close enough so that an orientational correlation exists. In this case the denominator in eq 16 becomes I_Bg_2 where g_2 is the static second rank orientational correlation factor.[107] In pure acetonitrile $g_2 > 1$ and therefore the initial curvature of $C_2(t)$ becomes smaller for collective rotation when compared to single-molecule rotation. It is reasonable to assume the same holds for dilute acetonitrile so that this effect does not explain our observation. Instead we assign the increased curvature mainly to librational motion. Remember that a librational oscillation was seen in the velocity correlation functions of Figure 10. It implies that rotation is not entirely free but modified by the librational potential, and the latter should contribute to the Einstein frequency, since it gauges all forces at $t = 0$.[117] The friction spectrum $\hat{\xi}_2(s)$ is therefore recalculated by using the scaled value $K_2(0) = 34.33$ ps^{-2}. For an empirical description it is fitted by Brownian oscillator relaxation functions in the frequency domain (Appendix A) of which four are required. It is more instructive to consider how the correlation function for the frictional torque decays in the time domain, hence $\xi_2(t)$ is shown in Figure 11b. Before further discussion we need to estimate how well $\xi_2(t)$ is determined and for this purpose retrace the analysis back to the OKE measurement. So first, by substitution of the fit to $\hat{\xi}_2(s)$ into eq 15, a description of $\hat{C}_2(s)$ is obtained. Next remember that the normalized response $R_L(t) = -dC_L(t)/dt$ has the transform

$$\chi_L(\omega) \equiv \hat{R}_L(s) = -s\hat{C}_L(s) + 1 \quad (19)$$

The measured spectral density is finally generated by multiplying $\chi_2''(\omega)$ from eq 19 with the measured spectral integral $S(t = 0) = 18.30$ (sum of pertinent amplitudes in Table 2). The result cannot be distinguished from the original spectrum on the scale of Figure 11a. The sensitivity of a BO parameter in $\xi_2(t)$ may be examined by calculating the standard deviation between simulated and measured data points. Optimal values and their likely errors (for which the standard deviation doubles from its minimum) represent the main result of this section and are summarized in Table 2.

The time-dependent rotational friction $\xi_2(t)$ will now be discussed in view of recent simulations.[19−21] As a first measure we consider the friction coefficient $\xi = \int_0^\infty \xi_2(t)\,\mathrm{d}t = \hat{\xi}(0) = 51.15\ \mathrm{ps}^{-1}$, which alone matters when friction decays much faster than the solute reorients. That condition may safely be assumed in the diffusive limit, i.e., when inertial motion has faded and solvent velocities are thermalized. There $C_\mathrm{L}(t)$ decays monoexponentially,

$$C_L(t) \approx \exp\{-L(L+1)D_r t\} \tag{20}$$

and the rotational diffusion constant D_r is given regardless of rank by

$$D_r = kT/I_B\xi \tag{21}$$

Kim and co-workers[20] simulated the molecular dynamics of polar model solutes in water and focused on the effect of solute polarizability. They determined $\xi = 7.6\ \mathrm{ps}^{-1}$ for a nonpolarizable solute with a 3.6-D dipole moment like acetonitrile, of which a major part ($5.6\ \mathrm{ps}^{-1}$) can be attributed to random torques from nonpolar interactions. When comparing simulated and observed ξ, one should rather consider the torque−torque correlation, the time integral of which scales with $I_B\xi$ according to eq 14. From our measurement for acetonitrile in water we find $\int_0^\infty \langle \vec{R}(0)\vec{R}(t)\rangle\,\mathrm{d}t = 2.95 \text{ x } 10^{-74}\ \mathrm{g}^2\ \mathrm{cm}^4\ \mathrm{ps}^{-3}$.[118] This result fits well into the range of values simulated with various solute models—for example, the nonpolarizable solute mentioned above gave $2.60 \text{ x } 10^{-74}\ \mathrm{g}^2\ \mathrm{cm}^4\ \mathrm{ps}^{-3}$.[20]

The shape should distinguish $\xi_2(t)$ from dynamic friction kernels of other rank. The function in Figure 11b can be well described by three exponentials:

$$\xi_2(t)/\mathrm{ps}^{-2} \approx 474 \exp\{-t/21.1\ \mathrm{fs}\} + 134 \exp\{-t/71.4\ \mathrm{fs}\} + 39.4 \exp\{-t/0.779\ \mathrm{ps}\}$$

which together represent 98% of the integral ξ. A small librational hump around 0.3 ps arises formally from the superposition of underdamped relaxation modes at 44 and 106 cm^{-1} (see Table 2). Interestingly, the simulated $\xi_1(t)$ (Figure 8a in ref 20) also appears to have a very weak second maximum at 0.2 ps. We note that while the *inertial* motion is properly presented by eqs 13 and 15, *librational* motion is not and therefore is projected into the friction kernel. Molecular dynamics simulations of time-dependent rotational friction in acetonitrile and methanol solutions found a pronounced quasi-Gaussian component within ∼100 fs, related to inertial solvent motions and accounting for more than 70% of the function's decay, followed by a small amplitude tail reflecting diffusive dynamics at longer times.[21] In particular for methanol, inertial motion was noted on two different time scales: a ∼100 fs time scale typical of small molecule liquids and the much faster ∼20 fs feature which was associated with hydroxyl librational motion. The ultrafast 21.1 fs component of our measurement may likewise be caused by water libration but intramolecular bending may also contribute. The longer time of 0.779 ps is assigned to translational motion of the acetonitrile solute coupled to collective orientational motions of the solvent as will be shown below. The oscillatory feature in $\xi_2(t)$ suggests backscattering from the solvent which may eventually be understood with mode-coupling theory.[119−121] The latter treats a solute rotating in a cage formed by a simple liquid, and the rotational friction is expanded into the modes of the entire system.

The theory of dielectric friction was developed from a molecular viewpoint by Madden and Kivelson.[18] For an analytical treatment the authors needed to assume separability between instantaneous near-range friction and slow-relaxing dipolar friction. As was already mentioned, molecular dynamics simulations showed that this assumption cannot be maintained.[20,21] We support that finding by showing that $\xi_2(t)$ curves generated from the dielectric theory never match, or do not describe qualitatively, the experimental curve at all times. To begin with, assume that a fraction $y\xi$ of the time integral can be considered δ-correlated. The corresponding rotational diffusion coefficient $D_0 = kT/I_\mathrm{B}y\xi$ is then entered into the dielectric part of $\xi_2(t)$ ($\xi_2^{\mathrm{DD}}(t)$ of eq 58 in ref 18a), which also contains functions from translational diffusion (for parameters see Table 1). The amplitude of $\xi_2^{\mathrm{DD}}(t)$ is determined so that integration gives the remaining fraction $(1 - y)\xi$. In Figure 11b, the curve which reproduces the slow decay time has $y = 0.3$; this means that the slow decay can be explained in terms of solute translational and water dielectric modes. On the other hand the observed friction at early times cannot be simulated even qualitatively by the theory since large differences remain in this region for every y. The integral of the predicted curve (grey area) is also too small since the remainder is reserved for D_0.

By the way the nuclear ^{14}N quadrupole coupling constant (NQCC) for dilute acetonitrile in water may be determined from our data. We calculate a correlation time $\tau_2^{(\mathrm{ACN})} = 1.49 \pm 0.015$ ps (at 21 °C), which is attributed to single-molecule reorientation. This property is usually inferred from the longitudinal magnetic relaxation time T_1 according to

$$\frac{1}{T_1} = \frac{3\pi^2}{2}\mathrm{NQCC}^2\ \tau_2^{(ACN)} \tag{22}$$

The problem is that even if accurate experimental NQR data exist, the coupling constant can differ from phase to phase (ref 122 and references therein). Using the solid-state value NQCC = 3.74 MHz,[123] Wakai et al.[55] obtain 2.29 ps for dilute $\mathrm{CD_3CN}$ in water at 20 °C, and after rescaling for $\mathrm{CH_3CN}$,[122] 2.20 ps is obtained without loss of accuracy. (This recent value is preferred to $\tau_2^{(\mathrm{ACN})} = 1.9$ ps, which was determined from line width measurement by Goldammer and Hertz.[124]) By comparison with our value, the appropriate coupling constant is found to be 4.54 ± 0.03 MHz, above the gas-phase value of 4.224 MHz.[125]

Compositional Dependence of Acetonitrile/Water DRS. Acetonitrile/water mixtures have been studied by a variety of methods including NMR,[55,69,122,126] Raman[57,127−129] and infrared spectroscopy,[113,130,131] dielectric relaxation,[58] far-infrared (fs THz) time domain spectroscopy,[59,132] X-ray diffraction,[131] as well as Monte Carlo[133] and molecular dynamics simulations.[126,134−137] (Here only the recent contributions are cited of the prolific literature from over 40 years.) Still many aspects of structural and dynamical properties of this binary remain to be unveiled, with the clearest picture coming from MD simulations. At issue is the proposed presence of microheterogeneity (ref 78 and references therein) raising fundamental questions about its concept and characterization. The spectroscopies referred to above including time-resolved OKE measurements[138] fail to address this issue directly because they access one-time correlation functions only. To be specific consider a mixture with acetonitrile mole fraction x_{ACN}. For any observable, the intermolecular spectral density may consist of "inhomogeneous broadening" from a static (or very slow) distribution of environments convoluted with "homogeneously broadened lineshapes" from the liquid dynamics. For deconvolution one must proceed to fifth order Raman experiments,[139−141] for example, which provide two-time correlation functions but are quite demanding theoretically[142] and experimentally,[143] since data from such experiments have proven difficult to interpret. But information on the liquid is also obtained if x_{ACN} is varied and the behavior of various (linear) spectral densities is charted and compared over a large compositional range. This is the route by which all experimentalists have so far examined the acetonitrile/water system.

Regarding DRS, the compositional dependence was shown in Figure 12 and parameters were given in Table 2. Combining femtosecond terahertz pulse spectroscopic results with thermodynamic arguments, Venables and Schmuttenmaer suggested that microheterogeneity seems questionable.[59] They found that the mixtures deviate from ideality most noticeably in the region between 0.10 and 0.40 acetonitrile mole fraction. The Debye model employed for describing the dielectric relaxation of the mixtures showed that they are better treated as uniform solutions rather than as two-component systems, so enhanced structure relative to ideal mixtures does not necessarily indicate microheterogeneity. In the same spirit, the composite and ACN "species" and their associated spectra in Figure 12 must be understood as an empirical description only. These data are best explained with the help of molecular dynamics simulations of the polarizability, which are only sparsely available at present.[126] This is why we defer a discussion of the line shape or the temporal behavior.

Here we comment first on the integral spectral density instead, which was shown in Figure 9 (empty circles); it is identical to the initial polarizability anisotropy $S^{(\mathrm{ACN})}(t = 0)$. In the range $x_{\mathrm{ACN}} < 0.5$, the initial signal appears to be somewhat larger than expected for independent acetonitrile solutes (solid line), which should have $S^{(1)}(t = 0) = 18.3x_{\mathrm{ACN}}$. Here the additional signal must come from the rank 2 orientational pair contribution, which therefore is positive,

$$0 < \sum_{j}^{N} \langle P_2[\vec{\Omega}_1(0)\cdot\vec{\Omega}_j(0)]\rangle \quad \text{with } 1 \neq j \tag{23}$$

indicating preferred parallel or antiparallel orientations at equilibrium. With higher mole fractions the initial signal becomes diminished compared even to rotationally independent acetonitrile molecules. This effect is assigned to collision-induced effects and for neat acetonitrile is consistent with molecular dynamics simulations.[107]

The second comment concerns the collective correlation time $\tau_2^{(\mathrm{ACN})}$ (solid circles). It increases from 1.49 ps at $x_{\mathrm{ACN}} = 0$ to 1.86 ps at $x_{\mathrm{ACN}} = 0.2$ and then falls again to 1.1 ps for neat acetonitrile. In ^{14}N nuclear quadrupole relaxation studies the single-molecule correlation time $\tau_2^{(\mathrm{ACN,\ s})}$ is determined instead. Wakai et al.[55] were able to cover the compositional range $2 \text{ x } 10^{-3} \leq x_{\mathrm{ACN}} \leq 2 \text{ x } 10^{-2}$, while Goldammer and Hertz[124] examined the range $5 \text{ x } 10^{-2} \leq x_{\mathrm{ACN}} \leq 1$. Taken together with our new NQCC for acetonitrile in water, $\tau_2^{(\mathrm{ACN,\ s})}$ is seen to be a constant 1.49 ps up to $x_{\mathrm{ACN}} \approx 0.15$, from where it decreases to 0.956 ps in neat acetonitrile.[122] It was already concluded that self-association of acetonitrile is not significant at small concentrations,[55,144] contrary to simulations.[134] Now it is tempting to see which information could be extracted from better data. For example, at $x_{\mathrm{can}} \approx 0.2$ we find at $t = 0$ that $S^{(\mathrm{ACN})}(0) = S^{(\mathrm{ACN,s})}(0) + S^{(\mathrm{ACN,\ p})}(0) \approx 1.11S^{(\mathrm{ACN,\ s})}(0)$. The measured correlation time $\tau_2 = 1.8$ ps may then be understood, according to eq 8, to be composed of $\tau_2^{(\mathrm{ACN,\ s})} = 1.49$ ps and a pair rotational correlation time $\tau_2^{(\mathrm{ACN,\ p})} \approx 3$ ps. This value is still subject to the uncertainties of our measurements at low x_{ACN}—the time dependence of the pair correlation should be a rewarding objective for future OKE and molecular dynamics studies.

Conclusion

Depolarized Rayleigh scattering (DRS) of acetonitrile/water mixtures at 21 °C was examined with the heterodyne-detected, time-resolved optical Kerr effect (OHD-OKE). A novel deconvolution method for materials with low nuclear response such as water was presented: a symmetric apparatus function is obtained from the rise of electronic response and an asymmetric correction is constructed with the help of high-frequency Raman data. Thus for the mixtures in the time domain, Raman spectra up to 1600 cm^{-1} were recorded with high signal/noise. Spectra are given relative to the water electronic response.

The DRS spectra for acetonitrile mole fraction $0.05 \leq x_{\mathrm{ACN}} \leq 1$ can be decomposed into three basic spectra with associated weight functions. The spectral density due to acetonitrile at infinite dilution in water was obtained by extrapolation. With the assumption of homogeneous broadening, it was transformed into the second rank reorientational relaxation function of single acetonitrile solutes. The Einstein frequency of 31.11 cm^{-1} is found higher than the thermal value of 27.11 cm^{-1} and an oscillation is observed in the corresponding velocity correlation function, both indicating librational motion in a solvent cage. Comparison of the rotational correlation time $\tau_2 = 1.49 \pm 0.015$ ps with NMR data for ^{14}N nuclear quadrupole relaxation gives a value 4.54 ± 0.03 MHz for the coupling constant. The reorientational correlation function is inverted to give the kernel for rotational friction. The latter is mainly described by exponentials with time constants of 21.05 fs, 71.4 fs, and 0.779 ps, which cannot be explained by the theory for dielectric friction. An oscillatory residue indicates coupling between acetonitrile libration and the water frictional modes.

Acknowledgment. We are grateful the Deutsche Forschungsgemeinschaft for generous support. Experimental assistance from S. Kovalenko is also acknowledged. This research has been supported by a Marie Curie Individual Fellowship (to G.M.P.) of the European Community under contract number HPMF-CT-2000-00775.

Appendix A

Different conventions are often used for integral transforms. We define the Fourier transform as $\mathrm{F}\{R(t)\} \equiv \int_{-\infty}^{+\infty} R(t)e^{i\omega}t\, \mathrm{d}t \equiv \chi(\omega) = \chi'(\omega) + i\chi''(\omega)$, which (since the response $R(t)$ vanishes before time zero) is identical to the Laplace transform $\mathrm{L}\{R(t)\} \equiv \int_0^{+\infty} R(t)e^{-st}\, \mathrm{d}t \equiv \hat{R}(s)$ with new variable $s = -i\omega$.

Consider the Laplace transform of a normalized relaxation function $C(t)$ (taken to be general so that the rank L which referred to orientational motion is omitted here). Its continued fraction expansion is truncated at the second order:

$$\hat{C}(s) = \cfrac{1}{s + \cfrac{K_0(0)}{s + \hat{\xi}(s)}} \tag{A1}$$

where $K_0(0)$ is the value of the velocity friction kernel at $t = 0$ and $\hat{\xi}(s)$ is the transform of the force friction kernel. With assumptions for the latter, special forms are created which are conveniently used to describe transient phenomena in the frequency and time domain. Generally, the response function $R(t) = -\mathrm{d}C(t)/\mathrm{d}t$ has the transform $\hat{R}(s) = -s\hat{C}(s) + 1$ and $\hat{R}(-i\omega) \equiv \chi(\omega)$.

Mori relaxation and line shape functions follow when the force friction kernel is set to decay exponentially, $\xi(t) = K_1(0)\exp\{-t/\tau_F\}$. In the frequency domain it is best to write

$$\hat{\xi}^{\mathrm{Mori}}(s) = \gamma\frac{1/\tau_F}{s + 1/\tau_F} \quad \text{with } \gamma = K_1(0)\tau_F \tag{A2}$$

Here γ constitutes a force friction or damping constant which is associated with the area-normalized decay. *Brownian Oscillator* functions[145,146] are obtained for delta-correlated force friction, that is in the limit $\tau_F \rightarrow 0$

$$\hat{\xi}^{BO}(s) = \gamma \tag{A3}$$

Next note that $\hat{C}(s)$ resembles $\mathscr{L}\{\cos(\omega_0 t)\}$. When the relaxation is expanded in t one has

$$C(t) = 1 - \frac{1}{2}{\omega_0}^2t^2 + ... \quad \text{with } {\omega_0}^2 = K_0(0) \tag{A4}$$

where ω_0 is the Einstein frequency. Using ω_0, γ, and τ_F for parameters, we obtain the Mori ($\tau_F > 0$) or BO ($\tau_F = 0$) functions

$$C'(\omega) = \gamma{\omega_0}^2/d$$

$$C''(\omega) = \omega[\gamma^2 + (1 + {\tau_F}^2\omega^2)(\omega^2 - {\omega_0}^2) - \gamma\tau_F(2\omega^2 - {\omega_0}^2)]/d \tag{A5}$$

$$\chi'(\omega) = {\omega_0}^2[\gamma\tau_F\omega^2 - (1 + {\tau_F}^2\omega^2)(\omega^2 - {\omega_0}^2)]/d$$

$$\chi''(\omega) = \omega\ {\omega_0}^2\gamma/\mathrm{d} \tag{A6}$$

with common denominator

$$d = \gamma^2\omega^2 + (1 + {\tau_F}^2\omega^2)(\omega^2 - {\omega_0}^2)^2 - 2\gamma\tau_F\omega^2(\omega^2 - {\omega_0}^2) \tag{A7}$$

The advantage of a multimode BO description is that all component relaxation and response functions can be given directly in the time domain. Here it is practical to distinguish the overdamped (od, $\omega_0 < \gamma/2$) or underdamped (ud, $\omega_0 > \gamma/2$) case:[146]

$$C^{(\mathrm{odBO})}(t) = \frac{1}{\lambda_1 - \lambda_2}[\lambda_1\exp\{-\lambda_2 t\} - \lambda_2\exp\{-\lambda_1 t\}] \quad \text{with } \lambda_{1/2} = \frac{1}{2}\gamma \pm \sqrt{(\gamma/2)^2 - {\omega_0}^2}$$

$$C^{(\mathrm{udBO})}(t) = \exp\{-\gamma t/2\}\left[\frac{\gamma}{2\Omega}\sin\{\Omega t\} + \cos\{\Omega t\}\right] \quad \text{with } \Omega = \sqrt{{\omega_0}^2 - (\gamma/2)^2} \tag{A8}$$

and the response functions are obtained as negative time derivatives.

Appendix B

The spectra are defined at M frequencies $\tilde{\nu}_i$ and for N acetonitrile mole fractions $x_j = 0, ..., 1$; the data may therefore be collected in a M x N matrix $\mathbf{D} = [\chi''_{\mathrm{nuc}}(\omega_i,x_j)]$. Note that the first column $|\mathbf{d}_1\rangle$ contains the spectrum of pure water. By SVD[110] the data can be written as

$$\mathbf{D} = \mathbf{U}\mathbf{S}\mathbf{V}^{\mathrm{T}} \tag{B1}$$

where the columns $|\mathbf{u}_k\rangle$ of $\mathbf{U}$ represent normalized basic spectra, the rows of $\mathbf{V}^{\mathrm{T}}$ contain their normalized dependence on x, and diagonal $\mathbf{S}$ has the weights or singular values $S_{kk} > 0$ arranged in descending order. Usually just a few (say K) such combinations adequately describe the data and $\mathbf{U}$, $\mathbf{S}$, and $\mathbf{V}^T$ are restricted to dimensions M x K, K x K, and K x N; in our case $K = 3$. Next the x-dependence is analyzed: the rows on $\mathbf{V}^{\mathrm{T}}$are approximated by linear combinations

$\mathbf{V}^{\mathrm{T}} \approx \mathbf{F}\mathbf{T}$ with target functions on

$$\mathbf{T} = \begin{bmatrix} 1 - x_j \\ x_j - (1 - x_j)^{\alpha}x_j^{\beta} \\ (1 - x_j)^{\alpha}x_j^{\beta} \end{bmatrix}_{j=1,N} \tag{B2}$$

Linear optimization without constraints is achieved analytically, for

$$\mathbf{F} = \mathbf{V}^{\mathrm{T}}\mathbf{T}^{\mathrm{T}}(\mathbf{T}\mathbf{T}^{\mathrm{T}})^{-1} \tag{B3}$$

The M x 3 matrix

$$\mathbf{B} = \mathbf{U}\mathbf{S}\mathbf{F} \tag{B4}$$

contains in its columns the spectra which are associated with $1 - x$, $x - (1 - x)^{\alpha}x^{\beta}$, and $(1 - x)^{\alpha}x^{\beta}$, respectively. However, we know already that the spectrum which contributes with weight $(1 - x)$ is identical to the water spectrum: $|\mathbf{d}_1\rangle$. This condition already determines the first column in $\mathbf{F}$

$$\mathbf{F}_{k1} = \langle\mathbf{u}_k|\mathbf{d}_1\rangle/S_{kk} \tag{B5}$$

and a different route must be followed to obtain the other coefficients. For this purpose we form $\mathbf{R}$ by deleting the first row of $\mathbf{T}$:

$$\mathbf{R} \equiv \begin{bmatrix} x_j - (1 - x_j)^{\alpha}x_j^{\beta} \\ (1 - x_j)^{\alpha}x_j^{\beta} \end{bmatrix}_{j=1,N} \tag{B6}$$

and solve for the remaining coefficients F_{kj} in

$$\mathbf{V}^{\mathrm{T}}\mathbf{R}^{\mathrm{T}} = \mathbf{F}\mathbf{T}\mathbf{R}^{\mathrm{T}} \tag{B7}$$

The associated spectra are again given by the columns of $\mathbf{B}$. Finally, the parameters α,β in $\mathbf{T}$ are optimized in the nonlinear part of the procedure, by minimizing $||\mathbf{V}^{\mathrm{T}} - \mathbf{F}\mathbf{T}||$.

References and Notes

(1) Kramers, H. A. *Physica* **1940**, *7*, 284.

(2) Steele, W. A. *Adv. Chem. Phys.* **1976,** *34*, 1−104.

(3) (a) Jang, J.; Stratt, R. M. *J. Chem. Phys.* **2000**, *112*, 7524−7537. (b) Jang, J.; Stratt, R. M. *J. Chem. Phys.* **2000**, *112*, 7538−7550.

(4) (a) Baskin, J. S.; Chachisvilis, M.; Gupta, M;.Zewail A. H. *J. Phys. Chem. A* **1998**, *102*, 4158−4171. (b) Baskin, J. S.; Zewail A. H. *J. Phys. Chem. A* **2001**, *105*, 3680−3692.

(5) (a) Chesnoy, J.; Gale, G. M. *Ann. Phys. (Paris)* **1984**, *9*, 893. (b) Chesnoy, J.; Gale, G. M. *Adv. Chem. Phys.* **1988**, *70* (2), 297−356.

(6) Owrutsky, J. C.; Raftery, D.; Hochstrasser, R. M. *Annu. Rev. Phys. Chem.*, **1994**, *45*, 519−555.

(7) Gnanakaran, S.; Hochstrasser, R. M. *J. Chem. Phys.* **1996**, *105*, 3486−3496.

(8) (a) Egorov, S. A.; Skinner, J. L. *J. Chem. Phys.* **1996**, *105*, 7047−7058. (b) Egorov, S. A.; Everitt, K. F.; Skinner, J. L. *J. Phys. Chem. A* **1999**, *103*, 9494−9499.

(9) Myers, D. J.; Shigeiwa, M.; Fayer, M. D.; Cherayil, B. J. *J. Phys. Chem. B* **2000**, *104*, 2402−2410.

(10) Schwarzer, D.; Teubner, M. *J. Chem. Phys*. **2002**, *116*, 5680−5693.

(11) Hansen, J. P.; McDonald, I. R. *Theory of Simple Liquids*; Academic Press Inc.: London, 1986.

(12) Zwanzig, R. In *Lectures in Theoretical Physics*; Britton, W. E., Downs, B. V., Downs, J., Eds.; Wiley-Interscience: New York, 1961; Vol. III; p 135.

(13) (a) Mori, H. *Prog. Theor. Phys. (Kyoto)* **1965**, *33*, 423. (b) Mori, H. *Prog. Theor. Phys. (Kyoto)* **1965**, *34*, 399.

(14) Grote, R. F.; Hynes, J. T. *J. Chem. Phys*. **1980**, *73*, 2715−2732.

(15) Hänggi, P.; Talkner, P.; Borkovec, M. *Rev. Mod. Phys*. **1990**, *62*, 251−341.

(16) In *Electron transfer- from isolated molecules to biomolecules;* Jortner, J., Bixon, M., Eds., *Adv. Chem. Phys*. **1990**, 106−107.

(17) Nee T. W.; Zwanzig, R. *J. Chem. Phys*. **1970**, *52*, 6353−6363.

(18) (a) Madden, P.; Kivelson, D. *J. Phys. Chem*. **1982**, *86*, 4244−4256. (b) Madden, P.; Kivelson, D. *Adv. Chem. Phys*. **1984,** *56*, 467−566.

(19) Papazyan, A.; Maroncelli, M. *J. Chem. Phys*. **1995**, *102*, 2888−2919.

(20) Bursulaya, B. D.; Zichi, D. A.; Kim, H. J. *J. Phys. Chem*. **1996**, *100*, 1392−1405.

(21) Kumar, P. V.; Maroncelli, M. *J. Chem. Phys*. **2000**, *112*, 5370−5381.

(22) Berkowitz, M.; Wan, W. *J. Chem. Phys*. **1987**, *86*, 376−382.

(23) Sridhar, G.; Vijayakumar, P.; Tembe, B. L. *J. Chem. Phys*. **1993**, *99*, 3147−3148.

(24) Das, A. K.; Madhusoodanan, M.; Tembe B. L. *J. Phys. Chem. A* **1997**, *101*, 2862−2872.

(25) Koneshan, S.; Lynden-Bell, R. M.; Rasaiah, J. C. *J. Am. Chem. Soc*. **1998**, *120*, 12 041−12 050.

(26) Das, A. K.; Tembe, B. L. *J. Mol. Liq*. **1998**, *77*, 131−156.

(27) Whitnell R. M.; Wilson K. R.; Hynes, J. T. *J. Chem. Phys*. **1992**, *96*, 5354−5369.

(28) Tuckerman, M.; Berne, B. J. *J. Chem. Phys*. **1993**, *98*, 7301−7318.

(29) Benjamin, I.; Whitnell, R. M. *Chem. Phys. Lett*., **1993**, *204*, 45−52.

(30) Bruehl, M.; Hynes, J. T. *Chem. Phys*. **1993**, *175*, 205−221.

(31) Wan, S. Z.; Xu, Y. W.; Wang, C. X.; Shi, Y. Y. *J. Chem. Phys*. **1995**, *102*, 4976−4980.

(32) Rey, R.; Hynes, J. T. *J. Chem. Phys*. **1998**, *108*, 142−153.

(33) Ladanyi, B. M.; Stratt, R. M. *J. Chem. Phys*. **1999**, *111*, 2008−2018.

(34) Wang, C. H. *Spectroscopy of condensed media, dynamics of molecular interactions*; Academic Press: London, 1985.

(35) Balucani, U.; Zoppi, M. *Dynamics of the Liquid State;* Clarendon Press: Oxford, U.K., 1994.

(36) In principle for NQR, in practice for dichroism, since measurements capture the diffusive limit only because of the large inertial moment of dyes.

(37) (a) Blanchard, G. J. *J. Phys. Chem*. **1988**, *92*, 6303−6307. (b) Blanchard, G. J. *J. Phys. Chem*. **1989**, *93*, 4315−4319. (c) Blanchard, G. J. *J. Phys. Chem*. **1991**, *95*, 5293−5299.

(38) Alavi, D. S.; Hartman, R. S.; Waldeck, D. H. *J. Chem. Phys*. **1991**, *94*, 4509−4520.

(39) van der Zwan, G.; Hynes, J. T. *J. Phys. Chem*. **1985**, *89*, 4181−4188.

(40) Kurnikova, M. G.; Waldeck, D. H.; Coalson, R. D. *J. Chem. Phys*. **1996**, *105*, 628−638.

(41) Balabai, N.; Sukharevsky, A.; Read, I.; Strazisar, B.; Kurnikova, M.; Hartman, R. S.; Coalson, R. D.; Waldeck, D. H. *J. Mol. Liq*. **1998**, *77*, 37−60.

(42) (a) Dutt, G. B.; Singh, M. K.; Sapre, A. V. *J. Chem. Phys*. **1998**, *109*, 5994−6003. (b) Dutt, G. B.; Ghanty, T. K.; Singh, M. K. *J. Chem. Phys*. **2001**, *115*, 10 845−10 851.

(43) Hartman, R. S.; Konitsky, W. M.; Waldeck, D. H.; Chang, Y. J.; Castner, E. W., Jr. *J. Chem. Phys*. **1997**, *106*, 7920−7930.

(44) Laitinen, E.; Korppi-Tommola, J.; Linnanto, J. *J. Chem. Phys*. **1997**, *107*, 7601−7612.

(45) (a) Dutt, G. B.; Krishna, G. R.; Raman, S. *J. Chem. Phys*. **2001**, 115, 4732−4741. (b) Dutt, G. B.; Raman, S. *J. Chem. Phys*. **2001**, *114*, 6702−6713.

(46) (a) Dutt, G. B.; Srivatsavoy, V. J. P.; Sapre, A. V. *J. Chem. Phys*. **1999**, *111*, 9705−9710. (b) Dutt, G. B.; Srivatsavoy, V. J. P.; Sapre, A. V. *J. Chem. Phys*. **1999**, *110*, 9623−9629.

(47) Wiemers, K.; Kauffman, J. F. *J. Phys. Chem. A* **2000**, *104*, 451−457.

(48) Dutt, G. B.; G. Rama Krishna, G. *J. Chem. Phys*. **2000**, *112*, 4676−4682.

(49) Dutt, G. B.; Ghanty, T. K. *J. Chem. Phys*. **2002**, *116*, 6687−6693.

(50) Hartman, R. S.; Waldeck, D. H. *J. Phys. Chem*. **1994,** *98*, 1386-1393.

(51) Srivastava, A.; Doraiswamy, S. *J. Chem. Phys*. **1995**, *103*, 6197−6205.

(52) Laia, C. A. T.; Costa, S. M. B. *Langmuir* **2002**, *18*, 1494−1504.

(53) Hartman, R. S.; Konitsky, W. M.; Waldeck, D. H. *J. Am. Chem. Soc*. **1993**, 115, 9692−9700.

(54) Balabai, N.; Waldeck, D. H. *J. Phys. Chem. B* **1997**, *101*, 2339−2347.

(55) Wakai, C.; Saito, H.; Matubayasi, N.; Nakahara, M. *J. Chem. Phys*. **2000**, *112*, 1462−1473.

(56) Jimenez, R.; Fleming, G. R.; Kumar, P. V.; Maroncelli, M. *Nature (London)* **1994**, *369* (6480*)*, 471−473.

(57) Reimers, J. R.; Hall, L. E. *J. Am. Chem. Soc.* **1999**, *121*, 3730−3744.

(58) Jellema, R.; Bulthuis, J.; van der Zwan, G. *J. Mol. Liq*. **1997**, *73*−*74*, 179−193.

(59) Venables, D. S.; Schmuttenmaer, C. A. *J. Chem. Phys*. **1998**, *108*, 4935−4944.

(60) Hickey, K.; Waghorne, W. E. *J. Chem. Eng. Data* **2001**, *46*, 851−857.

(61) Burnham, A. K.; Alms, G. R.; Flygare, W. H. *J. Chem. Phys*. **1975**, *62*, 3289−3297.

(62) Alms, G. R.; Burnham, A. K.; Flygare, W. H. *J. Chem. Phys*. **1975**, *63*, 3321−3326.

(63) Schwartz, M.; Wang, C. H. *Chem. Phys. Lett*. **1974**, *29*, 383−388.

(64) Kaatz, P.; Donley, E. A.; Shelton, D. P. *J. Chem. Phys*. **1998**, *108*, 849−856.

(65) Herzberg, G. *Molecular Spectra and Molecular Structure. II. Infrared and Raman Spectra of Polyatomic Molecules*; Krieger Publishing Company: Malabar, FL, original edition 1945, reprint edition with corrections 1991.

(66) Murphy, W. F. *J. Chem. Phys*. **1977**, *67*, 5877−5882.

(67) Huiszoon, C. *Mol. Phys*. **1986**, *58*, 865.

(68) Bien, T.; Possiel, M.; Doge, G.; Yarwood, J.; Arnold, K. E. *Chem. Phys*. **1981**, *56*, 203−211.

(69) Harris, K. R.; Newitt, P. J. *J. Phys. Chem. B* **1999**, *103*, 7015−7018.

(70) Hertz, H. G.; Leitner, H. *Z. Phys. Chem*. **1982**, *133*, 45.

(71) Ronne, C.; Thrane, L.; Astrand, P.-O.; Wallqvist, A.; Mikkelsen, K. V.; Keiding, S. R. *J. Chem. Phys*. **1997**, *107*, 5319−5331.

(72) McMorrow, D.; Lotshaw, W. T.; and Kenney-Wallace, G. A. *IEEE J. Quantum Electron*. **1988**, *24*, 443−454.

(73) Righini, R. *Science* **1993**, *262*, 1386−1390.

(74) Lotshaw, W. T.; McMorrow, D.; Thantu, N.; Melinger, J. S.; Kitchenham, R. *J. Raman Spectrosc*. **1995**, *26*, 571.

(75) McMorrow, D.; Thantu, N.; Kleiman, V.; Melinger, J. S.; Lotshaw, W. T. *J. Phys. Chem. A* **2001**, *105*, 7960−7972.

(76) Cho, M.; Du, M.; Scherer, N. F.; Fleming, G. R.; Mukamel, S. *J. Chem. Phys*. **1993**, *99*, 2410−2428.

(77) (a) Kinoshita, S.; Kai, Y.; Yamaguchi, M.; Yagi, T. *Phys. Rev. Lett*. **1995**, *75*, 148−151. (b) Kinoshita, S.; Kai, Y.; Yamaguchi, M.; Yagi, T. *Chem. Phys. Lett*. **1995**, *236*, 259−264.

(78) Marcus, Y.; Migron, Y. *J. Phys. Chem*. **1991**, *95*, 400−406.

(79) Walrafen, G. E. *J. Phys. Chem*. **1990**, *94*, 2237−2239.

(80) Palese, S.; Mukamel, S.; Dwayne Miller, R. J.; Lotshaw, W. T. *J. Phys. Chem*. **1996**, *100*, 10 380−10 388.

(81) Bartoli, F. J.; Litovitz, T. A. *J. Chem. Phys*. **1972**, *56*, 404.

(82) Patterson, G. D.; Griffiths, J. E. *J. Chem. Phys*. **1975**, 63, 2406−2413.

(83) Whittenburg, S. L.; Wang, C. H. *J. Chem. Phys*. **1977**, *66*, 4255−4262.

(84) Versmold, H.; *Ber. Bunsen-Ges. Phys. Chem*. **1978**, *82*, 451−457.

(85) Hilpert, R.; Langer, H.; Versmold, H. *Mol. Phys*., **1979**, 38, 2107−2110.

(86) Giorgini, M. G.; Morresi, A.; Cataliotti, R. S. *J. Raman Spectrosc*. **1995**, *26*, 601.

(87) Perova, T. S.; Vij, J. K. *J. Mol. Liq*. **1996**, *69*, 1−17.

(88) Blank, D. A.; Kaufman, L. J.; Fleming, G. R. *J. Chem. Phys*. **1999**, *111*, 3105−3114.

(89) One should distinguish $G_{\mathrm{sym}}(t)$ in Figure 2 and $G(t)$ in Figure 5, which are peak-normalized, from the corresponding area-normalized functions, which enter into deconvolution. We omit this distinction here to keep the notation simple.

(90) Deak, J. C.; Iwaki, L. K.; Dlott, D. D. *J. Phys. Chem*., **1998**, *102*, 8193−8201.

(91) Abramczyk, H.; Paradowska-Moszkowska, K. *Chem. Phys*. **2001**, *265*, 177−191.

(92) It is interesting that spectral structure appears in the blue wing of the 918 cm^{-1} band but not for neighboring bands. This could be due to a long 4.5-ps dephasing time (see: Morresi, A.; Sassi, P.; Paolantoni, M.; Santini, S.; Cataliotti, R. S. *Chem. Phys*. **2000**, *254*, 337−344) together with some small nonlinearity of our delay stage.

(93) McMorrow, D.; Lotshaw, W. T. *J. Phys. Chem*. **1991,** *95*, 10 395−10 406.

(94) Chang, Y. J.; Castner, E. W., Jr. *J. Chem. Phys*. **1993**, *99*, 113−125.

(95) Loughnane, B. J.; Scodinu, A.; Farrer, R. A.; Fourkas, J. T.; Mohanty, U. *J. Chem. Phys*. **1999**, *111*, 2686−2694.

(96) Castner, E. W., Jr.; Maroncelli, M. *J. Mol. Liq*. **1998**, *77*, 1−36.

(97) Ruthmann, J.; Kovalenko, S. A.; Ouw, D.; Ernsting, N. P. *J. Chem. Phys*. **1998**, *109*, 5466.

(98) Ohba, T.; Ikawa, S. *Mol. Phys*. **1991**, *73*, 985.

(99) Barthel, J.; Bachhuber, K.; Buchner, R.; Gill, J. B.; Kleebauer, M. *Chem. Phys. Lett*. **1990,** *167*, 62−66.

(100) Ladanyi, B. M.; Stratt, R. M. *J. Phys. Chem*. **1995**, *99*, 2502−2511.

(101) Kumar, P. V.; Maroncelli, M. *J. Chem. Phys*. **1995**, *103*, 3038−3060.

(102) Ladanyi, B. M.; Klein, S. *J. Chem. Phys*. **1996**, *105*, 1552−1561.

(103) Stratt, R. M.; Maroncelli, M. *J. Phys. Chem.* **1996**, *100*, 12981−12996.

(104) Ladanyi, B. M.; Maroncelli, M. *J. Chem. Phys*. **1998**, *109*, 3204−3221.

(105) Tassaing, T.; Danten, Y.; Besnard, M.; Zoïdis, E.; Yarwood, J. *Chem. Phys*. **1994**, *184*, 225−231.

(106) Hürth, M.; Woermann, D. *Ber. Bunsen-Ges. Phys. Chem*. **1987**, *91*, 614.

(107) Ladanyi, B. M.; Liang, Y. Q. *J. Chem. Phys*. **1995,** *103*, 6325−6332.

(108) The water spectrum is subtracted in its parametrized form given in Table 2.

(109) Flanders, B. N.; Cheville, R. A.; Grischkowsky, D.; Scherer, N. F. *J. Phys. Chem.* **1996**, *100*, 11 824−11 835.

(110) Press: W. H.; Teukolsky, S. A.; Vetterling, W. T.; Flannery, B. P. *Numerical Recipes in Fortran*, 2nd ed.; Cambridge Univerity Press: New York, 1992.

(111) Here the standard notation of Appendix B is used whenever possible; confusion of a target function $T_j(x)$ with an OHD-OKE trace $T(t)$ in the figures appears unlikely.

(112) (a) Morcom, K. W.; Smith, R. W. *J. Chem. Thermodyn*. **1969**, *1*, 503. (b) Stokes, R. H. *J. Chem. Thermodyn*. **1987**, *19*, 977−983. (c) Nakamura, M.; Tamura, K.; Muratami, S. *Thermochim. Acta*, **1995**, *253*, 127−136.

(113) Bertie, J. E.; Lan, Z. *J. Phys. Chem. B* **1997**, *101*, 4111−4119.

(114) Dunn III, W. J.; Nagy, P. I. *J. Phys. Chem*. **1990**, *94*, 2099−2105.

(115) Robertson, R. E.; Sugamori, S. E. *Can. J. Chem*. **1972**, *50*, 1353.

(116) Coffey, W. T.; Kalmykov, Y. P.; Waldron, J. T. *The Langevin Equation*; World Scientific: Singapore, 1996.

(117) Buchner, M.; Ladanyi, B. M.; Stratt, R. M. *J. Chem. Phys*. **1992**, *97*, 8522−8535.

(118) The scaled moment of inertia 91.2 (1−0.222) x 10^{-40} g cm^2 has been employed in eq 12.

(119) Götze, W. In *Liquids, Freezing and Glass Transition;* Les Houches Session LI, 1989; Hansen, J. P., Levesque, D., Zinn-Justin, J., Eds.; North-Holland: Amsterdam, 1991.

(120) Götze, W.; Sjögren, A. *Rep. Prog. Phys*. **1992**, *55*, 241−376.

(121) Bagchi, B.; Bhattacharyya, S. *Adv. Chem. Phys*. **2001**, *116*, 67−221.

(122) Hardy, E. H.; Zygar, A.; Zeidler, M. D. *Z. Phys. Chem*. **2000**, *214*, 1633−1657.

(123) (a) Gillen, K. T.; Noggle, J. H. *J. Chem. Phys*. **1970**, *53*, 801−809. (b) Negita, H.; Casabella, P. A.; Bray, P. J. *J. Chem. Phys*. **1960**, *32*, 314−315.

(124) Goldammer, E. v.; Hertz, H. G. *J. Phys. Chem*. **1970**, *74*, 3734−3755.

(125) Kukolich, S. G. *J. Chem. Phys*. **1982**, *76*, 97−101.

(126) Kovacs, H.; Laaksonen, A. *J. Am. Chem. Soc*. **1991**, *113*, 5596−5605.

(127) Rowlen, K. L.; Harris, J. M. *Anal. Chem.* **1991**, *63* (10), 964−969.

(128) Ulness, D. J.; Kirkwood, J. C.; Albrecht, A. C.; Stimson, M. J. *Asian J. Phys*. **1998**, *7*, 405−419.

(129) Holden, C. A.; Hunnicutt, S. S.; Rutan, S. C. *ACS, Division of Analytical Chemistry Abstracts*, 220th ACS National Meeting, Washington, DC, Aug 20−24, 2000; General Papers No. 50.

(130) Jamroz, D.; Stangret, J., Lindgren, J. *J. Am. Chem. Soc*. **1993**, *115*, 6165−6168.

(131) Takamuku, T.; Tabata, M.; Yamaguchi, A.; Nishimoto, J.; Kumamoto, M.; Wakita, H.; Yamaguchi, T. *J. Phys. Chem. B* **1998**, *102*, 8880−8888.

(132) Venables, D. S.; Schmuttenmaer, C. A. *J. Chem. Phys*. **2000**, *113*, 11 222−11 236.

(133) Satoh, Y.; Nakanishi, K. *Fluid Phase Equilib.* **1995**, *104*, 41−55.

(134) Matsumoto, M.; Tanaka, H.; Nakanishi, K. *J. Chem. Phys*. **1993**, *99*, 6935−6940.

(135) Bergman, D. L.; Laaksonen, A. *Phys. Rev. E* **1998**, *58*, 4706−4715.

(136) Molinero, V.; Laria, D.; Kapral, R. *J. Chem. Phys*. **1998**, *109*, 6844−6853.

(137) (a) Mountain, R. A. *J. Phys. Chem. A* **1999**, *103*, 10 744−10 748. (b) Mountain, R. A. *J. Phys. Chem. B* **2001**, *105*, 6556−6561.

(138) Tanimura, Y.; Mukamel, S. *J. Chem. Phys*. **1993**, *99*, 9496−9511.

(139) (a) Tominaga, K.; Yoshihara, K. *J. Chem. Phys*. **1996**, *104*, 1159−1162. (b) Tominaga, K.; Yoshihara, K. *J. Chem. Phys*. **1996**, *104*, 4419−4426.

(140) Steffen, T.; Duppen, K. *Phys. Rev. Lett*. **1996**, *76*, 1224−1227.

(141) Tokmakoff, A.; Fleming, G. R. *J. Chem. Phys*. **1997**, *106*, 2569−2582.

(142) Mukamel, S.; Piryatinski, A.; Chernyak, V. *Acc. Chem. Res*. **1999**, *32*, 145−154.

(143) (a) Blank, D. A.; Kaufman, L. J.; Fleming, G. R. *J. Chem. Phys*. **2000**, *113*, 771−778. (b) Kaufman, L. J.; Blank, D. A.; Fleming, G. R. *J. Chem. Phys*. **2001**, *114*, 2312−2331.

(144) Kovacs, H.; Kowalewski, J.; Maliniak, A. *Chem. Phys. Lett.* **1988**, *152*, 427−430.

(145) Risken, H. *The Fokker−Planck Equation*, 2nd ed.; Springer: Berlin, 1989.

(146) Mukamel, S. *Principles of Nonlinear Optical Spectroscopy*; Oxford University Press: New York, 1995.